Predicted impacts of heterogeneous chemical pathways on particulate sulfur over Fairbanks, Alaska, the N. Hemisphere, and the Contiguous United States

Sara Farrell[1,2,3], Havala O. T. Pye[2], Robert Gilliam[2], George Pouliot[2], Deanna Huff[4], Golam Sarwar[2], William Vizuete[1], Nicole Briggs[5], Kathleen Fahey[2]

1. Department of Environmental Science and Engineering, The University of North Carolina at Chapel Hill, Chapel Hill, NC 27516, USA

2. Office of Research and Development, U.S. Environmental Protection Agency, Research Triangle Park, Durham, NC 27709, USA

3. Oak Ridge Institute for Science and Education, U.S. Environmental Protection Agency, Research Triangle Park, NC 27709, USA

4. Alaska Department of Environmental Conservation, P.O. Box 111800, Juneau, 99811-1800

5. Laboratory Services and Applied Sciences Division at USEPA, Region 10, Seattle, WA 98101

Correspondence to: Kathleen Fahey (Fahey.Kathleen@epa.gov) and Sara Farrell (Farrell.Sara@epa.gov)

Abstract. A portion of Alaska's Fairbanks North Star Borough was designated as nonattainment for the 2006 24-hour $PM_{2.5}$ National Ambient Air Quality Standard (NAAQS) in 2009. $PM_{2.5}$ NAAQS exceedances in Fairbanks mainly occur during the dark and cold winters, when temperature inversions form and trap high emissions at the surface. Sulfate (SO_4^{2-}), often the second largest contributor to $PM_{2.5}$ mass during these wintertime PM episodes, is underpredicted by atmospheric chemical transport models (CTMs). Most CTMs account for primary SO_4^{2-}, and secondary SO_4^{2-} formed via gas-phase oxidation of sulfur dioxide (SO_2) and in-cloud aqueous oxidation of dissolved S(IV). Dissolution and reaction of SO_2 in aqueous aerosols is generally not included in CTMs but can be represented as heterogeneous reactive uptake and may help better represent the high SO_4^{2-} concentrations observed during Fairbanks winters. In addition, hydroxymethanesulfonate (HMS), a particulate sulfur species sometimes misidentified as SO_4^{2-}, is known to form during Fairbanks winters. Heterogeneous formation of SO_4^{2-} and HMS in aerosol liquid water (ALW) was implemented in the Community Multiscale Air Quality (CMAQ) modeling system. CMAQ simulations were performed for wintertime PM episodes in Fairbanks (2008) as well as over the N. Hemisphere and Contiguous United States (CONUS) for 2015-2016. The added heterogeneous sulfur chemistry reduced model mean sulfate bias by ~0.6 µg/m³ during a cold winter PM episode in Fairbanks, AK. Improvements in model performance are also seen in Beijing, during wintertime haze events (reducing model mean sulfate bias by ~2.9 µgS/m³). This additional sulfur chemistry also improves modeled summertime SO_4^{2-} bias in the southeast U.S. with implications of future modeling of biogenic organosulfates.

1 Introduction

Radiative forcing and climate effects attributed to $PM_{2.5}$ (fine particulate matter 2.5 µm or less in diameter) remain among the most uncertain in climate change assessments (IPCC, 2013). Acute and long-term exposure to $PM_{2.5}$ has been associated with

negative health outcomes including, but not limited to, acute myocardial infarction, stroke, and respiratory complications (Chen et al., 2018; Hayes et al., 2020; Silva et al., 2016; USEPA, 2019; Yang et al., 2021; Yitshak-Sade et al., 2018). Some of the most extreme $PM_{2.5}$ episodes in history have occurred when inverted vertical temperature profiles cause stable atmospheric conditions that limit pollution dilution (Holzworth, 1972; Malek et al., 2006; Scott, 1953; Wallace and Kanaroglou, 2009). Near surface temperature inversions (with a minimum modeled planetary boundary layer height of 1.7m) are characteristic of Fairbanks and North Pole, Alaska winters, and are associated with degraded air quality in this region (Malingowski et al., 2014; Mayfield and Fochesatto, 2013). Wintertime $PM_{2.5}$ episodes have impacted human health in these cities (McLaughlin, 2010), with this region exceeding the National Ambient Air Quality Standards (NAAQS) for $PM_{2.5}$ since 2009, when portions of the Fairbanks North Star Borough were designated as nonattainment for the 2006 24-hour $PM_{2.5}$ NAAQS[1] (ADEC, 2017, 2019).

Sulfate (SO_4^{2-}), often a major component of $PM_{2.5}$ in Fairbanks and North Pole (ADEC, 2017) as well as globally (Snider et al., 2016), can be emitted directly (primary) or formed secondarily via atmospheric oxidation of sulfur dioxide (SO_2). Known secondary SO_4^{2-} formation processes include but are not limited to gas phase oxidation of SO_2 (Calvert et al., 1978), particle surface oxidation of SO_2 (Clements et al., 2013; Wang et al., 2021), and in-cloud aqueous-phase oxidation of inorganic sulfur species with oxidation number 4 (S(IV) = $SO_2 \cdot H_2O + HSO_3^- + SO_3^{2-}$) (secondary) (Hoffmann and Calvert, 1985; Ibusuki and Takeuchi, 1987; Lagrange et al., 1994; Lee and Schwartz, 1983a; Maahs, 1983; Maaß et al., 1999; Martin and Good, 1991; McArdle and Hoffmann, 1983). Aside from contributing directly to $PM_{2.5}$ mass, SO_4^{2-} can facilitate the formation of other $PM_{2.5}$ species as a reactant (Brüggemann et al., 2020; Huang et al., 2019; Huang et al., 2020; Surratt et al., 2010), by increasing aerosol water uptake (Kim et al., 1994; Nguyen et al., 2014), and by altering aerosol acidity (Li et al., 2022; Pye et al., 2020).

Under heavily polluted haze conditions, such as those common in the North China Plain during the winter, recent studies have suggested that secondary SO_4^{2-} may be efficiently produced in aerosol liquid water (ALW) (Cheng et al., 2016; Fan et al., 2020; Liu et al., 2020). Hygroscopic $PM_{2.5}$ (both inorganic and organic) can increase ALW content (Nguyen et al., 2014; Petters and Kreidenweis, 2007; Pye et al., 2017), which can facilitate secondary SO_4^{2-} formation (Zhang et al., 2021a), enhancing SO_4^{2-} concentrations in a positive feedback loop – which is particularly important during high relative humidity haze events (Cheng et al., 2016; Song et al., 2021b; Wang et al., 2016; Wang et al., 2014).

---

[1] The United States Clean Air Act requires EPA to set National Ambient Air Quality Standards (NAAQS) for six pollutants including fine particulate matter (PM2.5) and to periodically review those standards. In 2006, EPA updated the NAAQS for PM2.5 concentrations averaged over a 24-hour time period. This updated standard requires the calculation of the 98th percentile of daily (24-hour) PM2.5 concentrations for three years, and that the average of those three 98th percentile concentrations be at or below a threshold of 35 ug/m3. For simplicity, we refer to this as the 2006 24-hour PM2.5 NAAQS.

60 Chemical transport models generally include secondary SO_4^{2-} formation via gas-phase oxidation of SO_2 by OH, and in-cloud aqueous-phase oxidation of dissolved S(IV) species by oxidants such as hydrogen peroxide (H_2O_2), ozone (O_3), peroxyacetic acid (PAA), methyl hydroperoxide (MHP), and/or oxygen (O_2) catalyzed by transition metal ions (TMI-O_2), iron (Fe^{3+}) and manganese (Mn^{2+}). Limited to these formation pathways, CTMs have been unable to reproduce the high levels of SO_4^{2-} observed during wintertime PM events in Beijing and the sub-Arctic. This persistent underprediction suggests that CTMs are

65 lacking SO_4^{2-} formation pathways that take place when photochemistry and cloud liquid water are limited (Eckhardt et al., 2015; Gao et al., 2016; Wang et al., 2014). Previous studies have suggested that heterogeneous sulfate formation in deliquesced aerosol particles may account for at least part of this underprediction (Wang et al., 2014; Zheng et al., 2015). Wang et al. (2014) implemented generalized heterogeneous reactive uptake of SO_2 to form SO_4^{2-} (where relative humidity-dependent uptake coefficients were specified rather than calculated) in the GEOS-Chem global model (Chen et al., 2009), and this led to

70 improved model-observation comparisons for SO_4^{2-} during a wintertime haze event over North China (Wang et al., 2014). Similarly, when Zheng et al. (2015) implemented generalized heterogeneous sulfur chemistry in WRF-CMAQ, the SO_4^{2-} normalized mean bias decreased from -54.2% to 6.3% for Beijing haze events (Zheng et al., 2015).

The inclusion of hydroxymethanesulfonate (HMS) chemistry in CTMs may also ameliorate negative model bias. General SO_4^{2-}

75 PM measurement methods struggle to disentangle SO_4^{2-} spectra from that of inorganic S(IV) and HMS (Dovrou et al., 2019). HMS is formed from the aqueous-phase reaction of S(IV) with formaldehyde (HCHO) (Boyce and Hoffmann, 1984; Deister et al., 1986; Kok et al., 1986; Kovacs et al., 2005; Olson and Hoffmann, 1986). Recent field, modeling, and experimental studies have highlighted the importance of secondary SO_4^{2-} and HMS formation in aqueous aerosols during wintertime haze events (Campbell et al., 2022; Dovrou et al., 2019; Ma et al., 2020; Moch et al., 2020; Song et al., 2019). Moch et al. (2020)

80 suggested up to 25% of measured SO_4^{2-} may actually be HMS in heavily polluted regions. Arctic and sub-arctic winter conditions may favor HMS formation, as colder temperatures increase the solubility of SO_2 and HCHO, and limited sunlight reduces the photo-oxidation of HCHO (Moch et al., 2020; Pandis and Seinfeld, 1989; Sander, 2015; Song et al., 2019; Staudinger and Roberts, 1996). In the work of Song et al. (2021) including generalized heterogeneous cloud HMS chemistry in GEOS-Chem reduced model-measurement differences in HMS/SO_4^{2-} ratios. The inclusion of heterogeneous formation and

85 loss of HMS in deliquesced aerosols increased modelled HMS concentrations, particularly in China (Song et al., 2021a).

Exploring heterogeneous sulfur chemistry in deliquesced aerosols requires retrofitting of multi-phase reactions. Many laboratory studies characterizing rate coefficients and expressions for aqueous phase SO_4^{2-} formation were performed under dilute conditions, characteristic of cloud droplets. The ionic strength of aerosol particles, however, can be several orders of

90 magnitude higher than that of cloud droplets due to aerosols containing much lower concentrations of water (Mekic and Gligorovski, 2021). Ionic strength has been found to impact the aqueous-phase formation of SO_4^{2-}, increasing the rate of aqueous-phase kinetics for NO_2 and H_2O_2 oxidation of S(IV) (Chen et al., 2019; Liu et al., 2020) and inhibiting the aqueous-

phase kinetics of TMI-catalyzed O_2 oxidation (Ibusuki and Takeuchi, 1987; Martin and Good, 1991; Martin and Hill, 1987). Experimental studies have also shown that high ionic strength may increase or decrease (effective) Henry's law coefficients

95 of reactants compared to pure water (Ali et al., 2014; Chen et al., 2019; Kosak-Channing and Helz, 1983; Lagrange et al., 1994; Liu et al., 2020; Millero et al., 1989; Shao et al., 2019).

In this paper we describe the implementation of heterogenous sulfur chemistry in ALW in the Community Multiscale Air Quality (CMAQv5.3.2) modeling system (USEPA, 2020), leading to additional SO_4^{2-} and HMS formation. We refer to this

100 chemistry as heterogeneous given the use of the heterogeneous framework (Hanson et al., 1994). Heterogeneous sulfur chemistry pathways implemented include the oxidation of dissolved S(IV) species by H_2O_2, O_3, PAA, MHP, TMI-O_2, NO_2, and the in-aerosol aqueous formation of HMS. In addition to heterogeneous chemistry updates, ionic strength effects were added to condensed-phase rate expressions and Henry's law coefficients of some species. The updated model was applied for several time periods and for different domains and horizonal resolutions. Two historical wintertime PM episodes were

105 simulated for a finely resolved (1.33 km) domain centered over Fairbanks, Alaska, winter and summer periods over the contiguous United States (CONUS) (12 km) during 2016, and the 2015-2016 winter season over the N. hemisphere (108 km) to investigate the impacts of these updates for different chemical regimes, domains, and seasons. Changes to SO_4^{2-}, HMS, and SO_4^{2-} + HMS (PM$_{2.5,sulf}$) predictions were tracked with each update (i.e., for (1) adding heterogeneous sulfur reactions and (2) adding ionic strength effects), and model performance was evaluated with available observations. This study aims to better

110 understand the impacts that heterogeneous sulfur chemistry parameterizations may have on predicted PM$_{2.5,sulf}$ concentrations and whether the additional chemistry can resolve SO_4^{2-} underpredictions in cold and dark conditions.

2 Methods

2.1 Heterogeneous Sulfur Chemistry

115 In this study, reactions that transform SO_2 to SO_4^{2-} and HMS are simulated in both cloud and ALW. In ALW, the production of particulate SO_4^{2-} and HMS is parameterized as a set of first-order heterogeneous reactions of SO_2 (gas) or reactants (e.g., HCHO, O_3, NO_2, etc.) as follows:

$$P_{SO2,reactant} \xrightarrow{k_{het}} \text{PM}_{2.5,sulf} \qquad \qquad \text{(Reaction. 1)}$$

Where PM$_{2.5,sulf}$ refers to both sulfate and HMS and k_{het} is the heterogeneous rate constant (Eq. 1), which accounts for gas-to-

120 particle mass transfer processes, aqueous reactive uptake and sulfur transformations (Jacob, 2000).

$$k_{het}(s^{-1}) = \frac{SA}{\frac{r_p}{D_g} + \frac{4}{v\gamma}} \qquad \text{(Eq. 1)}$$

where SA is the aerosol surface area (m^2/m^3), r_p is the effective particle radius (m), D_g is gas-phase diffusivity of a reactant (m^2/s), and v is the mean molecular speed of the partitioning gas (m/s). γ is the reactive uptake coefficient and is given by the following equation (Hanson et al., 1994; Jacob, 2000; Schwartz, 1986):

125

$$\gamma = \left[\frac{1}{\alpha} + \frac{v}{4HRT\sqrt{D_a k_{chem}}} \cdot \frac{1}{\coth(q) - \frac{1}{q}}\right]^{-1} \qquad \text{(Eq. 2)}$$

where α is the mass accommodation coefficient of a species, H is the effective Henry's law coefficient (M/atm) at temperature T (K), R is the ideal gas constant, 0.08206 (L·atm/mol·K), D_a is the aqueous-phase diffusivity (assumed here as 10^{-9} m^2/s), k_{chem} represents the pseudo-first order condensed-phase rate coefficient (s^{-1}) (Table 1), and q is the diffuso-reactive parameter defined as $q = r_p\sqrt{\frac{k_{chem}}{D_a}}$ (Schwartz and Freiberg, 1981). The rate expressions in aerosol water for the base configuration

130 (hereafter referred to as "Base_Het") are the same as those used for cloud chemistry (Appel et al., 2017; Sarwar et al., 2013). Heterogeneous sulfur chemistry was calculated when relative humidity (RH) was greater than or equal 50% following Shao et al. (2019), assuming that below a 50% RH, the aerosol water content would be too low for heterogeneous sulfur chemistry to take place (Sun et al., 2013). The heterogeneous chemistry is also solved simultaneously with gas-phase chemistry.

2.2 Accounting for ionic strength effects and alternative chemical rate expressions

135 Several studies have investigated the impact of high ionic strength on sulfate oxidation rates originally developed for dilute conditions. Depending on reaction pathway, rates may be enhanced or diminished with increased ionic strength (Chen et al., 2019; Lagrange et al., 1994; Liu et al., 2020; Shao et al., 2019). Ionic strength is calculated in CMAQ as:

$$I = \frac{1}{2}\sum_{i=1}^{n} m_i z_i^2 \qquad \text{(Eq. 3)}$$

where m_i is the solute concentration (M) in aerosol or cloud liquid water and z_i is the charge associated with each modelled

140 ion.

SO$_2$ can be oxidized in the aqueous phase by O$_2$ when catalyzed by TMI (specifically Fe^{3+} and Mn^{2+}) with synergies existing when both Fe^{3+} and Mn^{2+} are present (Altwicker and Nass, 1983; Ibusuki and Takeuchi, 1987; Martin and Good, 1991). This reaction pathway has been found to be an important secondary SO$_4^{2-}$ formation pathway, especially at low pH and when

145   photochemistry is limited and Fe is more soluble (Cheng et al., 2016; Li et al., 2020; Liu et al., 2022; Song et al., 2021b). Ibusuki and Takeuchi (1987) found that the rate of S(IV) oxidation by the TMI-O_2 pathway peaked around pH = 4.2, decreased with decreased temperature, and was enhanced by high concentrations of TMI (Ibusuki and Takeuchi, 1987). Martin and Good investigated the impact of higher S(IV) concentrations on this SO_4^{2-} formation pathway and found that higher S(IV) concentrations alter the rates of catalysis via Fe^{3+} and Mn^{2+} along with their synergistic catalysis and did not explore a pH nor

150   temperature dependency (Martin and Good, 1991). However, at similar pH ranges, S(IV) and soluble Fe^{3+} and Mn^{2+} concentrations, Martin and Good found that their rate expression agreed well with that by Ibusuki and Takeuchi (Ibusuki and Takeuchi, 1987; Martin and Good, 1991). When Shao et al. (2019) implemented the Ibusuki-Takeuchi TMI-catalyzed O_2 oxidation rate expression in ALW in GEOS-Chem, they found that this pathway accounted for 67-69% of SO_4^{2-} formed over China (Shao et al., 2019). The presence of higher S(IV) concentrations, however, may warrant the use of a SO_4^{2-} formation

155   rate that takes into consideration faster rates of TMI catalysis (Martin and Good, 1991). The TMI-O_2 oxidation pathway from Martin and Good (1991) is used in the "Base_Het" simulation and the TMI-O_2 oxidation pathway from Ibusuki and Takeuchi (1987) is used in the "TMI_sens" simulation to explore the range in SO_4^{2-} formation possible by this pathway (Table 1). For both implementations of this pathway, ionic strength impacts were added as high ionic strength has been found to limit the TMI-catalyzed oxidation of S(IV) to SO_4^{2-} (Martin and Hill, 1967; Martin and Hill, 1987).

160   While the TMI-catalyzed oxidation pathway can be a significant contributor to secondary SO_4^{2-} formation, especially at low pH, some studies suggest SO_4^{2-} formation during Beijing winter haze events may be dominated by the reaction of SO_2 and NO_2 in aerosol and/or cloud and fog water under mildly acidic or neutral conditions (Cheng et al., 2016; Wang et al., 2020; Yang et al., 2019). This oxidation pathway may increase in importance with increasing ionic strength (Cheng et al., 2016). Recent chamber work by Chen et al. (2019) found that increasing ionic strength increased the rate of secondary SO_4^{2-} formation

165   from NO_2 oxidation (Chen et al., 2019). To assess the potential impact ionic strength may have on this pathway, the ionic strength dependent NO_2 oxidation rate of Chen et al., (2019) was included in the "TMI_NO2" sensitivity simulation (Table 1).

    While the aforementioned pathways are pH dependent, SO_2 aqueous oxidation by H_2O_2 is pH independent for pH > 2 due to the opposing dependencies of the reaction rate coefficient and S(IV) solubility on pH (Clifton et al., 1988; Seinfeld and Pandis,

170   2016). This pathway has been studied extensively in dilute conditions representative of cloud droplets (Hoffmann and Calvert, 1985; Maaß et al., 1999; McArdle and Hoffmann, 1983). Maaß et al. (1999) found that oxidation of S(IV) by H_2O_2 increases with increased ionic strength and formulated a semi-empirical relationship between ionic strength and the reaction rate coefficient for the S(IV)-H_2O_2 oxidation pathway (upper limit of ionic strength in this study = 5M) (Maaß et al., 1999). Field measurements during Chinese haze events have reported ionic strengths of aerosols ranging from 14-43 M (Cheng et al., 2016;

175   Fountoukis and Nenes, 2007). Liu et al. (2020) recently studied this pathway using aerosol flow reactors to determine an ionic strength-based enhancement factor that encapsulates the combined ionic strength effects on Henry's law coefficients, dissociation, and condensed-phase kinetics. This study found that increasing ionic strength from 0 to 14 M resulted in an order-of-magnitude increase in SO_4^{2-} production rate (Liu et al., 2020).

180   O_3 is another important aqueous-phase oxidant of SO_2 with a reaction rate that increases with increasing pH (Maahs, 1983) and ionic strength (Lagrange et al., 1994). The ionic strength enhancement factor for this rate has been implemented with other ionic strength enhancement or inhibition factors in the "All_Ionic" sensitivity simulation (Table 1).

Table 1. Pseudo-first-order rate constants (k_{chem}) and ionic strength (I) factors for each simulation.

Uptake gas	Model Simulation	k_{chem} (s^{-1})	Product	Reference
O_3	Base_Het, TMI_sens, TMI_NO2_sens	$k_{O3} = k_1[H_2SO_3] + k_2[HSO_3^-] + k_3[SO_3^{2-}]$ $k_1 = 2.4 \times 10^4 \text{ M}^{-1}\text{s}^{-1}$ $k_2 = 3.7 \times 10^5 \times e^{-5530 \times \left(\frac{1}{T} - \frac{1}{298}\right)} \text{ M}^{-1}\text{s}^{-1}$ $k_3 = 1.5 \times 10^9 \times e^{-5280 \times \left(\frac{1}{T} - \frac{1}{298}\right)} \text{ M}^{-1}\text{s}^{-1}$	SO_4^{2-}	(Hoffmann and Calvert, 1985)
	All_Ionic	$k_{O3,I} = k_{O3} \times (1 + (b \times I_{O_3}))$ $I_{O_3,max} = 1.2 \text{ M}$ $b = 1.94$[a]	SO_4^{2-}	(Lagrange et al., 1994)
H_2O_2	Base_Het, TMI_sens, TMI_NO2_sens	$k_{H2O2} = \frac{k_4[H^+][HSO_3^-]}{1 + K[H^+]}$ $k_4 = 7.45 \times 10^7 \times e^{-4430 \times \left(\frac{1}{T} - \frac{1}{298}\right)} \text{ M}^{-1}\text{s}^{-1}$ $K = 13 \text{M}^{-1}$	SO_4^{2-}	(McArdle and Hoffmann, 1983)
	All_Ionic	$k_{H2O2,I} = k_4 \times [HSO_3^-] \times [H^+] \times$ $10^{\,0.36 I_{H_2O_2} - \frac{1.018\sqrt{I_{H_2O_2}}}{1 + 0.17\sqrt{I_{H_2O_2}}}}$ $k_4 = 9.1 \times 10^7 \times e^{-3572 \times \left(\frac{1}{T} - \frac{1}{298}\right)} \text{ M}^{-1}\text{s}^{-1}$ $I_{H_2O_2,max} = 5\text{M}$	SO_4^{2-}	(Maaß et al., 1999)
NO_2	Base_Het, TMI_sens	$k_{NO2} = k_5[S(IV)]$ [b] $k_5 = 2 \times 10^6 \text{ M}^{-1}\text{s}^{-1}$	SO_4^{2-}	(Lee and Schwartz, 1983b)
	TMI_NO2_sens, All_Ionic	$k_{NO2,I} = k_{5,ionic}[S(IV)]$ [b]	SO_4^{2-}	(Chen et al., 2019)

		$k_{5,ionic} = 10^{6.1+\frac{3.1\times I_{NO_2}}{I_{NO_2}+0.2}}$ $I_{NO_2,max} = 1.14M$		
SO₂	Base_Het	$k_{TMIO2,I} =$ $\frac{k_6[\text{Mn(II)}]+k_7[\text{Fe(III)}]+k_8[\text{Mn(II)}][\text{Fe(III)}]}{1+75\times S(VI)_S^{0.67}} \times$ $10^{b\times\frac{\sqrt{I_{TMI}}}{1+\sqrt{I_{TMI}}}}$ $k_6 = 750 \text{ M}^{-1}\text{s}^{-1}$ $k_7 = 2600 \text{ M}^{-1}\text{s}^{-1}$ $k_8 = 1e^{10}\text{M}^{-2}\text{s}^{-1}$ $I_{TMI,max} = 2M$ $b = -4.07$ [c]	SO_4^{2-}	(Martin and Good, 1991) (Martin and Hill, 1987)
	TMI_sens, TMI_NO2_sens, All_Ionic	$k_{TMIO2,I} = k_6[\text{H}^+]^{-0.74}[\text{Mn(II)}][\text{Fe(III)}]$ $(for \text{ pH} \leq 4.2)$ $k_6 = 3.72 \times 10^7 \times e^{-8431.6\times\left(\frac{1}{T}-\frac{1}{297}\right)} \times$ $10^{b\times\frac{\sqrt{I_{TMI}}}{1+\sqrt{I_{TMI}}}} \text{ M}^{-2}\text{s}^{-1}$ $k_{TMIO2,I} = k_7[\text{H}^+]^{0.67}[\text{Mn(II)}][\text{Fe(III)}]$ $(for \text{ pH} > 4.2)$ $k_7 = 2.51 \times 10^{13} \times e^{-8431.6\times\left(\frac{1}{T}-\frac{1}{297}\right)} \times$ $10^{b\times\frac{\sqrt{I_{TMI}}}{1+\sqrt{I_{TMI}}}} \text{ M}^{-2}\text{s}^{-1}$ $I_{TMI,max} = 2M$ $b = -4.07$ [c]	SO_4^{2-}	(Ibusuki and Takeuchi, 1987) (Martin and Hill, 1987)
HCHO[d]	Base_Het, TMI_sens, TMI_NO2_sens All_Ionic	$k_8[\text{HSO}_3^-] + k_9[\text{SO}_3^{2-}]$ $k_8 = 790 \times e^{-2900\times\left(\frac{1}{T}-\frac{1}{298}\right)}$ $k_9 = 2.5 \times 10^7 \times e^{-2450\times\left(\frac{1}{T}-\frac{1}{298}\right)}$	HMS	(Boyce and Hoffmann, 1984)

185 [a] The ionic strength cap chosen corresponds with the activation energy for rate constant, k_1, which matches the ionic strength cap, b, for sodium perchlorate (NaClO₄).

[b] $[S(IV)](M) = [\text{SO}_2\cdot\text{H}_2\text{O}] + [\text{HSO}_3^-] + [\text{SO}_3^{2-}]$

Table 2. Henry's law coefficients used per model simulation.

Species	Model Simulation	H_A (M atm^{-1})	Reference
O_3	Base_Het TMI_sens TMI_NO2_sens	$H_{O_3}^{I_{O_3}=0} = 0.0114 \times e^{2300 \times (\frac{1}{T}-\frac{1}{298})}$	(Kosak-Channing and Helz, 1983)
	All_Ionic	$H_{O_3} = e^{\frac{2297}{T}-2.659 \times I_{O_3}+688 \times \frac{I_{O_3}}{T}-12.19}$ $I_{O_3,max} = 0.6\ M$	(Kosak-Channing and Helz, 1983)
H_2O_2	Base_Het TMI_sens TMI_NO2_sens	$H_{H_2O_2}^{I_{H_2O_2}=0} = 1.1 \times 10^5 \times e^{7400 \times (\frac{1}{T}-\frac{1}{298})}$	(O'Sullivan et al., 1996)
	All_Ionic	$H_{H_2O_2}^{I_{H_2O_2}=0} = 1.3 \times 10^5 \times e^{7300 \times (\frac{1}{T}-\frac{1}{298})}$ $\frac{H_{H_2O_2}}{H_{H_2O_2}^{I_{H_2O_2}=0}} = 1 - 1.414 \times 10^{-3} \times I_{H_2O_2}^2 + 0.121 I_{H_2O_2}$ $I_{H_2O_2,max} = 5M$	(Seinfeld and Pandis, 2016) (Ali et al., 2014; Liu et al., 2020)
NO_2	Base_Het, TMI_sens TMI_NO2_sens All_Ionic	$H_{NO_2} = 0.012 \times e^{2500 \times (\frac{1}{T}-\frac{1}{298})}$	(Chameides, 1984)
SO_2	Base_Het TMI_sens TMI_NO2_sens	$[H_2SO_3] = H_{SO_2} \times p_{SO_2}$ $[HSO_3^-] = K_{a1} \times [H_2SO_3]/[H^+]$	(Lide et al., 1995)

		$[SO_3^{2-}] = K_{a2} \times [HSO_3^-]/[H^+]$ $H_{SO_2} = 1.4 \times e^{2900 \times (\frac{1}{T} - \frac{1}{298})}$ $K_{a1} = 0.013 \times e^{1960 \times (\frac{1}{T} - \frac{1}{298})}$ $K_{a2} = 6.6 \times 10^{-8} \times e^{1500 \times (\frac{1}{T} - \frac{1}{298})}$	
	All_Ionic [a]	$H_{SO_2}^{I_{SO_2}=0} = 1.2 \times e^{3100 \times (\frac{1}{T} - \frac{1}{298})}$ $\frac{H_{SO_2}}{H_{SO_2}^{I_{SO_2}=0}} = 10^{((\frac{22.3}{T} - 0.0997) \times I_{SO_2})}$ $K_{a1}^I = K_{a1} \times 10^{0.5\sqrt{I} - 0.31I}$ $K_{a2}^I = K_{a2} \times 10^{1.052\sqrt{I} - 0.36I}$ $I_{SO_2,max} = 6\ \text{M}$	(Seinfeld and Pandis, 2016) (Millero et al., 1989)
HCHO	Base_Het, TMI_sens TMI_NO2_sens All_Ionic	$H_{HCHO} = \frac{H_{HCHO}^*}{1 + K_{HCHO}^{HYD}}$ $H_{HCHO}^* = 3200 \times e^{6800 \times (\frac{1}{T} - \frac{1}{298})}$ $K_{HCHO}^{HYD} = \frac{0.18 \times e^{4030 \times (\frac{1}{T} - \frac{1}{298})} \times 55.5M}{0.0051}$	(Seinfeld and Pandis, 2016) (Ervens et al., 2003; Staudinger and Roberts, 1996)

[a] Aqueous phase concentrations of S(IV) are calculated similarly to the Base_Het, TMI_sens, and TMI_NO2_sens but with

200   ionic-strength dependent equilibrium coefficients.

For the fine mode aerosol, total gas + particle concentrations of key inorganic species are passed to the thermodynamic equilibrium model, ISORROPIA II, to calculate aerosol pH and ALW (Fountoukis and Nenes, 2007). In addition to the ALW associated with inorganic ions, ALW associated with organic aerosols are also estimated in CMAQ via hygroscopicity

205   parameters (Pye et al., 2017).

2.3 Model base case and sensitivity simulations

Several CMAQ configurations were used here to understand the impacts of adding heterogeneous sulfur chemistry, ionic strength, and the use of alternative pseudo-first order rate expressions. A base case CMAQ simulation ("Base") was completed

210   using in-cloud SO_4^{2-} formation from aqueous oxidation by H_2O_2, O_3, PAA, MHP, and via TMI-catalyzed O_2 of SO_2 and gas-phase oxidation of SO_2 by OH (Fahey et al., 2017; Sarwar et al., 2013).

To account for the impacts of heterogeneous sulfur chemistry in ALW, the Base_Het model simulation was completed for all domains (see Model Configuration) using the aforementioned heterogenous reactive uptake parameterizations (Eq. 1-2).

215   Parameters from CMAQ's KMT2 cloud chemistry model (Fahey et al., 2017; Fahey and Roselle, 2019) were used to calculate k_{chem} (Table 1). An ionic strength inhibition term was added to the TMI-catalyzed O_2 pathway in aerosol water to account for the limiting effect of ionic strength on this pathway. The ionic strength was capped at I_{max} = 2 M to reflect experimental constraints (Martin and Good, 1991; Martin and Hill, 1987; Seinfeld and Pandis, 2016). For this pathway in both cloud and ALW, Fe^{3+} was assumed to be 90% of dissolved Fe at night and 10% during the daytime, with soluble fractions of Mn and Fe

220   assumed to be 0.5 and 0.1 of total Fe and Mn respectively (Alexander et al., 2009). Other sources of less soluble Fe and Mn emissions, such as dust, are likely minimal given snow-cover for this domain and episode (Shao et al., 2019).

The k_{chem} for the TMI-catalyzed O_2 pathway in the Base_Het case is neither temperature nor pH dependent (Martin and Good, 1991; Martin and Hill, 1987). Ibusuki and Takeuchi (1987) found both a pH and temperature dependence on the k_{chem} for this

225   pathway (Ibusuki and Takeuchi, 1987; Martin and Hill, 1987). To explore the effects of both a pH and temperature dependences on the rate of TMI-catalyzed sulfur oxidation pathway, a sensitivity simulation, "TMI_sens", was run (Ibusuki and Takeuchi, 1987). Given that this k_{chem} is reduced in colder temperatures, the TMI_sens run likely represents a lower bound on SO_4^{2-} formation for this pathway during winter episodes. This k_{chem} also uses the same solubility, dissociation and ionic strength bounds as the TMI-catalyzed O_2 oxidation pathway used in the Base_Het simulation.

230

In the "TMI_NO2_sens" simulations both the alternative k_{chem} for the TMI-catalyzed O_2 pathway and an ionic strength-dependent k_{chem} for the NO_2 oxidation pathway in ALW are included (Chen et al., 2019; Ibusuki and Takeuchi, 1987). Both the TMI-O_2 and the NO_2 oxidation k_{chem}'s favor weakly acidic pH regimes (Cheng et al., 2016; Martin and Good, 1991). This sensitivity simulation was implemented to analyze potential competition between two pathways under their favorable pH

235   conditions, and that are also characteristic of winter-time haze episodes (weakly acidic) (Cheng et al., 2016).
Ionic strength impacts on k_{chem} for H_2O_2 and O_3 aqueous oxidation formation pathways were included on top of the previous modifications in the TMI_sens and TMI_NO2_sens model simulations (Chen et al., 2019; Ibusuki and Takeuchi, 1987; Maaß et al., 1999). Ionic strength adjustments were also included for S(IV) dissociation constants and Henry's law coefficients for H_2O_2, O_3 and SO_2 in the "All_Ionic" simulations (Ali et al., 2014; Lagrange et al., 1994; Maaß et al., 1999; Millero et al.,

240   1989; Seinfeld and Pandis, 2016) to analyze the combined effects of ionic strength on total modelled $PM_{2.5,sulf}$ aerosol.

In addition to the reactions shown in Table 1 (which are treated in both aerosol and cloud water), also included is S(IV) oxidation by peroxyacetic acid (PAA) and methyl hydroperoxide (MHP) in aerosol and cloud water and in-cloud S(IV)

oxidation by HNO_4, OH and NO_3 (Lee and Schwartz, 1983a; Lind et al., 1987; Martin, 1984). With the exception of the "Base" case which used CMAQ's default "AQCHEM" cloud chemistry, all other simulations used the KMT2 cloud chemistry scheme. KMT2 includes additional inorganic and organic chemistry compared to AQCHEM, including several additional S(IV) oxidation reactions as well as HMS formation and loss.

2.4 Model Configuration

Results of base and sensitivity simulations were compared for three different spatial domains: Fairbanks, Alaska, the contiguous U.S (CONUS), and the Northern Hemisphere. Model simulations over Fairbanks and North Pole, Alaska, span two wintertime PM episodes (Episode 1 (E1): Jan 25th-Feb 11th, 2008 and Episode 2 (E2): Nov 4th-Nov 17th, 2008) with two days of spin-up and a horizontal resolution of 1.33 km. Model simulations over the Northern Hemispheric domain were performed for the winter season from Dec 2015 - Feb 2016 with 2 months of spin-up and a horizontal resolution of 108 km following a standard US EPA configuration described by (Mathur et al., 2017) and (Appel et al., 2021). Model simulations over the CONUS domain were run for the months of January and July 2016 with 10 days of spin up and at a horizontal resolution of 12km.

The Weather Research and Forecasting model (WRF (Skamarock et al., 2008)) was used to develop meteorology on all three domains. The Fairbanks WRF case follows the original configuration and case study of Gaudet et al. (2010, 2012) for Fairbanks, AK. This older WRF simulation was updated from WRFv3.3 (Gaudet, 2010, 2012) to WRFv4.1.1. with all geophysical and meteorological inputs reprocessed for compatibility with the more recent version of WRF and using the Mellor-Yamada-Nakanishi-Niino 2.5 order closure scheme (MYNN2.5 (Nakanishi and Niino, 2009)). Sensitivity testing found performance improvements when updating the planetary boundary layer model change from the Mellor-Yamada-Janjić (MYJ) scheme to MYNN2.5. Evaluations also showed that the WRFv4.1.1 configuration captured the extreme temperature variations in these cases well, with 2-m temperature root mean square error (RMSE) on the order of 2-3 K, which is within historical benchmarks for complex geographical areas that are more difficult to model (Kemball-Cook et al., 2005). For the CONUS, meteorological inputs were sourced from WRFv4.1.1 and CMAQ-inputs were processed with the Meteorology-Chemistry interface processor (MCIP (Appel et al., 2017; Otte and Pleim, 2010)) version 5.0.

The emissions inputs for the two Fairbanks wintertime PM episodes were based on inputs provided by the Alaska Department of Environmental Conservation (ADEC). These emission estimates were from the base year (2008) used for the Fairbanks $PM_{2.5}$ Moderate State Implementation Plan (SIP) and represent the best available emission estimates for the two time periods. Table 5.6-3 from section 5.06 of (ADEC, 2014) provides a summary of the methods and inputs used to develop this emission inventory. For this model set up, we used the same inventory inputs and scripts and only updated the speciation for CMAQv5.3.2. The emission inventories for the Northern Hemispheric domain follow the same setup as described in (Appel

12

et al., 2021) where anthropogenic emissions were sourced from the 2010 Hemispheric Transport for Air Pollution version 2 (Janssens-Maenhout et al., 2015), biogenic emissions were sourced from the Model of Emissions of Gases and Aerosols from Nature (Guenther et al., 2012), soil and lightning NO were sourced from the Global Emissions Initiative (http://www.geiacenter.org), biomass burning emissions were sourced from the Fire Inventory from National Center for Atmospheric Research (Wiedinmyer et al., 2011), and onroad and nonroad emissions were developed using the Motor Vehicle Emission Simulator v2014a. The emission inventories for the CONUS domain were sourced from the 2016 modeling platform 2016v7.2 (beta and Regional Haze) Platform (which is documented at https://views.cira.colostate.edu//wiki/wiki/10197 and used in (Appel et al., 2021).

Gas-phase chemistry was simulated using the CB6r3 mechanism (Luecken et al., 2019) and aerosol dynamics were simulated using the aero7 module. Boundary conditions for the Fairbanks domain were sourced from the EPA's Air QUAlity TimE Series Project (EQUATES) for 2008 (USEPA, 2021). The sulfur tracking method (STM) (which is documented at https://github.com/USEPA/CMAQ/blob/main/DOCS/Users_Guide/CMAQ_UG_ch12_sulfur_tracking.md and used in (Fahey and Roselle, 2019)) was extended to include the new heterogeneous sulfur chemical pathways in order to track the contributions of each chemical reaction, primary emissions, and initial and boundary conditions to modelled SO_4^{2-} (Appel et al., 2021).

2.5 Sulfate and PM$_{2.5,sulf}$ Observations

The model predictions were evaluated against available observations. While most monitoring networks report measurements for PM$_{2.5}$ or PM$_1$ SO_4^{2-}, recent studies have indicated hydroxymethanesulfonate may be included in those observations (Dovrou et al., 2019; Ma et al., 2020; Moch et al., 2018; Song et al., 2019). Based on these findings, we compare measured SO_4^{2-} to modelled PM$_{2.5,sulf}$:

$$PM_{2.5,sulf} \left(\frac{\mu g}{m^3}\right) = SO_4^{2-} + HMS \times \frac{MW_{SO_4^{2-}}}{MW_{HMS}}$$ (Eq. 4)

PM$_{2.5}$ SO_4^{2-} observations in Fairbanks during 2008 were obtained from ADEC's Therma Electron Partisol 2000, single channel instrument w/SCC monitor 020900010 (State Office Building in Fairbanks Alaska; 64.840672, -147.722461) (ADEC, 2023). SO_4^{2-} observations for the 2016 Hemispheric Domain were sourced from the United States Environmental Protection Agency (USEPA) Air Quality System (AQS) monitoring network, the Canadian National Air Pollution Surveillance (NAP) monitoring network, the European Monitoring and Evaluation Programme (EMEP) monitoring network, and one monitor at Tsinghua University in Beijing, China (ECCC, 2022; Ma et al., 2020; Tørseth et al., 2012; USEPA). Modelled PM$_{2.5,sulf}$ concentrations and measured SO_4^{2-} from the AQS and NAP networks were cast in units of micrograms sulfur per meter cubed ($\mu gS/m^3$) to match the measurement units used in the EMEP and Tsinghua University SO_4^{2-} measurements.

13

3 Results

3.1 Modelled particulate sulfur enhancement during dark and cold PM episodes in Fairbanks and North Pole, AK

3.1.1 Aerosol sulfur enhancements during a wintertime haze event (Episode 1 (E1))

The Base simulation average E1 sulfate concentrations around Fairbanks and North Pole, AK are ~ 2 - 3.5 mg/m^3 (Fig. 1a and c). Compared to the Base, the Base_Het simulation leads to increased $PM_{2.5,sulf}$ predictions concentrated around the cities of Fairbanks and North Pole as well as the region south of the Tanana River (Figure 1b, d). The additional heterogeneous chemistry in the Base_Het simulation contributes up to an additional 11 µg/m^3 of maximum daily $PM_{2.5,sulf}$ compared to the Base simulation in the region south of the Tanana River. Maximum daily differences are defined as:

$$Maximum\ Daily\ Differences = \max(Avg_{daily,2} - Avg_{daily,1}) \qquad \text{(Eq. 5)}$$

Enhancements in $PM_{2.5,sulf}$ concentrations for the Base_Het simulation are mainly driven by increases in SO_4^{2-} concentrations (increasing up to 10.9 µg/m^3 for daily maximum differences across the entire domain), with lesser impacts from HMS (increasing up to ~1 µg/m^3 for daily maximum differences across the entire domain). HMS concentrations are enhanced more in North Pole than Fairbanks, coinciding with higher HCHO emissions (Fig. S1) from residential wood combustion combined with high co-located SO_2 emissions (from home heating oil) along with lower temperatures (ADEC, 2017).

14
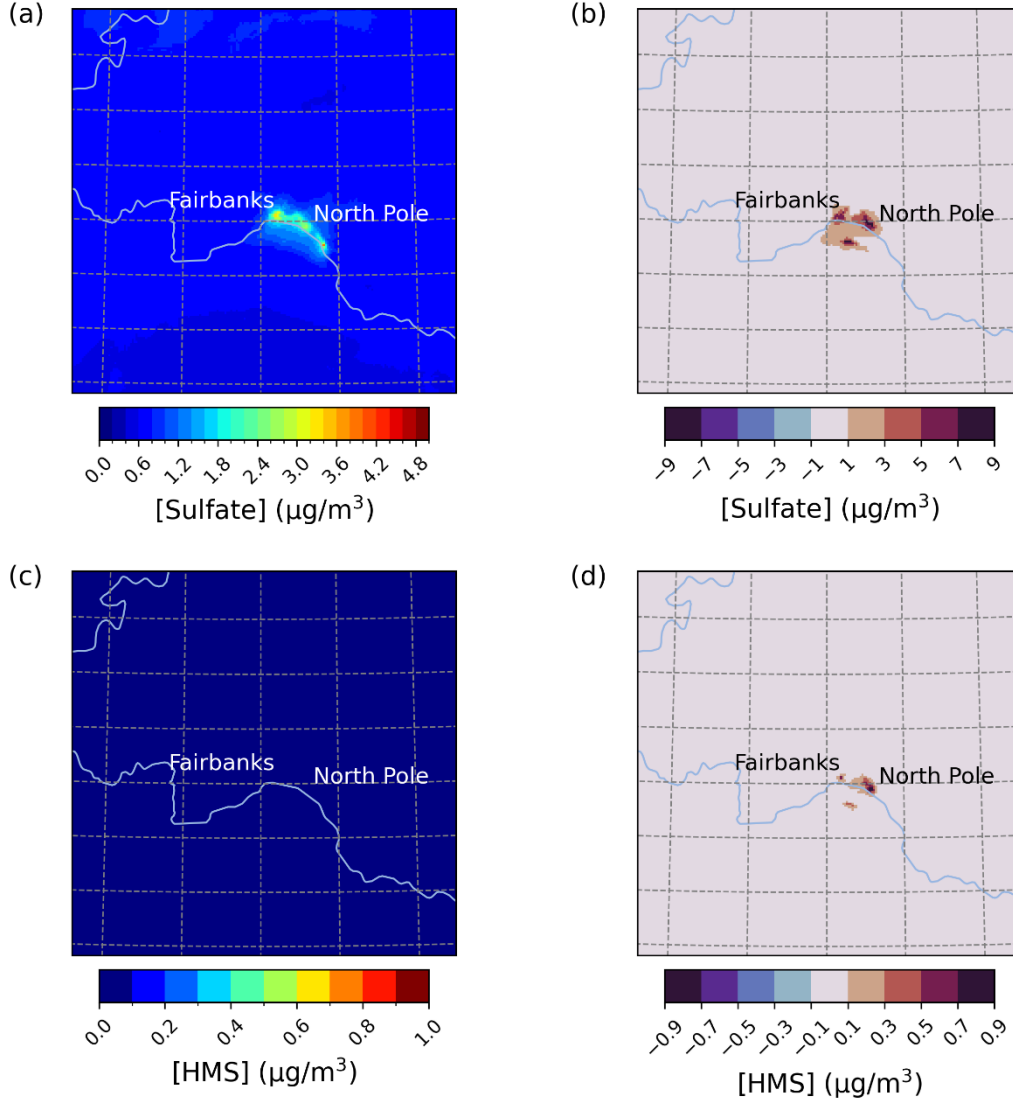
Figure 1: Episode average sulfate (a), and HMS (c) concentrations in the Base simulation along with daily max differences in sulfate (b), and HMS (d) concentrations between the Base_Het and Base CMAQ simulations over Fairbanks and North Pole AK for episode 1 (from January 25th, 2008, to February 11th, 2008). HMS formation was not included in Base CMAQ (i.e., HMS = 0 in the Base simulation). Domain size is 264.67 km by 264.67 km with a grid cell resolution of 1.33 km by 1.33 km.

Out of all of the secondary $PM_{2.5,sulf}$ formation pathways that are enhanced during dark cold conditions (TMI-catalyzed O_2,

335   NO_2, and the formation of HMS), the leading secondary SO_4^{2-} formation pathway in the Base_Het is the TMI-catalyzed O_2 oxidation pathway in ALW (Fig. 2). The first order condensed phase rate constant (k_{chem}) of this pathway is lower than that of the k_{chem} for NO_2 by almost 2 orders of magnitude for average modeled conditions characteristic of Fairbanks and North Pole for E1 (aerosol pH = 3.83, [Fe(III)] = 0.24 M, [Mn(II)] = 0.002 M, [SO_2] = 20 ppb, [NO2] = 20 ppb, [SO_4^{2-}] = 3 µg/m³, [ALW] = 6 µg/m³, and Temp = 243K) (Fig. S2) and is ~ 1 order of magnitude higher than that for HMS formation in ALW.

340   Despite the NO_2 k_{chem} being higher, the TMI-catalyzed O_2 heterogeneous rate of sulfate formation is dependent upon SO_2 partitioning into the particle, as Fe and Mn are both aerosol species, and simulated dark conditions reduce the conversion of Fe^{3+} to Fe^{2+} from daytime photochemical reactions (Alexander et al., 2009; Rao and Collett, 1998; Shao et al., 2019). The effective Henry's law coefficient for SO_2 increases with pH, while the Henry's law coefficient for NO_2 remains low across the pH spectrum. This and a higher mass accommodation coefficient (by ~2 orders of magnitude) for SO_2 compared to NO_2

345   contribute to the TMI-catalyzed O_2 pathway outcompeting the NO_2 pathway for this model configuration. The TMI-catalyzed O_2 heterogeneous reactive uptake pathway also outcompetes the H_2O_2 and O_3 heterogeneous reactive uptake pathways due to low photochemical activity with the dark conditions of this domain and episode.

The formation of HMS is higher in North Pole, which can be colder than Fairbanks by up to ~5°C. Higher modelled HCHO

350   emissions in North Pole (Fig. S1) along with colder temperatures, increase the partitioning of HCHO onto existing particles This effect and the increase in HMS formation is more pronounced in the TMI_sens simulation (Fig. S3 a and b).

Compared to the k_{chem} used in Base_Het, the alternative k_{chem} in the TMI_sens for the TMI-catalyzed O$_2$ pathway is ~2 orders of magnitude lower under average conditions characteristic of this episode (Fig. S2) with the extremely cold temperatures decreasing the TMI-catalyzed O$_2$ oxidation k_{chem}. This ultimately results in a slower conversion of S(IV) species to SO$_4^{2-}$ and subsequent competition with HMS formation, which increases with colder temperatures (Fig. S4). Maximum daily average enhancements in modelled PM$_{2.5,sulf}$ concentrations in the TMI_sens simulation reach up to 25 µg/m^3 at a grid cell in North Pole and are mostly attributed to high HMS concentrations (Fig. S3 a and b). Formation rates of HMS are also dependent on aerosol pH, which can be higher at North Pole than in Fairbanks (Fig. S4). Higher pH increases the conversion of HSO$_3^-$ to SO$_3^{2-}$ and the rate constant for HCHO reaction with SO$_3^{2-}$ is 5 orders of magnitude higher than that of the reaction with HSO$_3^-$ (Boyce and Hoffmann, 1984). Lower SO$_4^{2-}$ production rates in TMI_sens and lower modelled aerosol acidity compared to Base_Het likely contributes to the higher HMS formation (and loss) rates seen in the TMI_sens simulation. It is important to note that while aerosol acidity is modified by aqueous-phase formation of SO$_4^{2-}$, it is not modified by the formation of HMS in CMAQ.

When implementing an ionic strength dependent NO$_2$ rate expression (Chen et al., 2019) on top of this alternative TMI-catalyzed O$_2$ rate expression in the "TMI_NO2_sens" model simulation, the NO$_2$ oxidation pathway outcompeted the formation of HMS (Fig. S3). While this model simulation compared well with the Base_Het model simulation in daily averaged PM$_{2.5,sulf}$ concentrations, it predicted significantly lower PM$_{2.5,sulf}$ concentrations than the TMI_sens in North Pole due to a reduction in HMS predicted. Compared to downtown Fairbanks, North Pole has lower NO$_2$ emissions but the switch to the ionic-strength dependent reaction rate still leads to higher SO$_4^{2-}$ production in North Pole compared to TMI_sens.

The "ALL_Ionic" model simulation resulted in similar PM$_{2.5,sulf}$ predictions and pathway contributions as the TMI_NO2_sens simulation for this episode (Fig. S3). In both Fairbanks and North Pole, SO$_4^{2-}$ formation attributed to heterogeneous reactive uptake via the H$_2$O$_2$ oxidation pathway increased slightly. For ionic strength factor calculations, ionic strength is capped at the maximum ionic strength considered in the experiments the parameterizations are based on (~5-6M) (Ali et al., 2014; Millero et al., 1989). The modelled ionic strength of ALW is typically at or above the maximum experimental ionic strength when deriving both the effective Henry's law coefficients, dissociation coefficients, and k_{chem} for the H$_2$O$_2$ oxidation pathway – leading to expected higher dissolution and kinetics for this pathway. HMS concentrations for this model simulation also increased slightly in comparison to the TMI_NO2_sens. Assuming excess of dark oxidant pre-cursors (TMI, NO$_2$ and HCHO) and maximum ionic strength, the leading higher HMS production rate in the ALL_Ionic is likely due to a slightly higher range of aerosol pH (~2-5.5) compared to the Base_Het and TMI_NO2_sens simulations (Fig. S3d).

3.1.2 Aerosol sulfur enhancements with liquid cloud events (episode 2 (E2))

Sulfate and HMS are known to form efficiently in cloud and fog droplets (Altwicker and Nass, 1983; Boyce and Hoffmann, 1984; Calvert et al., 1978; Clifton et al., 1988; Ibusuki and Takeuchi, 1987; Lee and Schwartz, 1983a; Martin and Good, 1991; McArdle and Hoffmann, 1983). In E1, there was minimal cloud or fog liquid water simulated; however, during E2 (November 4 – November 11, 2008), there were some periods where cloud/fog chemistry impacts on $PM_{25,sulf}$ formation were evident.

Compared to E1, $PM_{2.5,sulf}$ concentration enhancements were lower overall during E2. Differences between Base_Het and Base simulations, however, are appreciable during this episode with $PM_{2.5,sulf}$ increasing up to 4.6 µg/m^3 across the entire domain (daily maximum difference) (Fig. 3). Enhancements in $PM_{2.5,sulf}$ are mainly driven by increased SO_4^{2-} formation in and around Fairbanks and North Pole; however, simulated HMS concentrations reached up to 4.4 µg/m^3 south of the Tanana River (daily maximum) for this episode. Note that the Base simulation included some contributions from in-cloud S(IV) oxidation (i.e., 5 S(IV) oxidation reactions from CMAQ's default cloud chemistry mechanism (AQCHEM)), while Base_Het includes the additional in-cloud chemical reactions from the KMT2 cloud chemistry module.
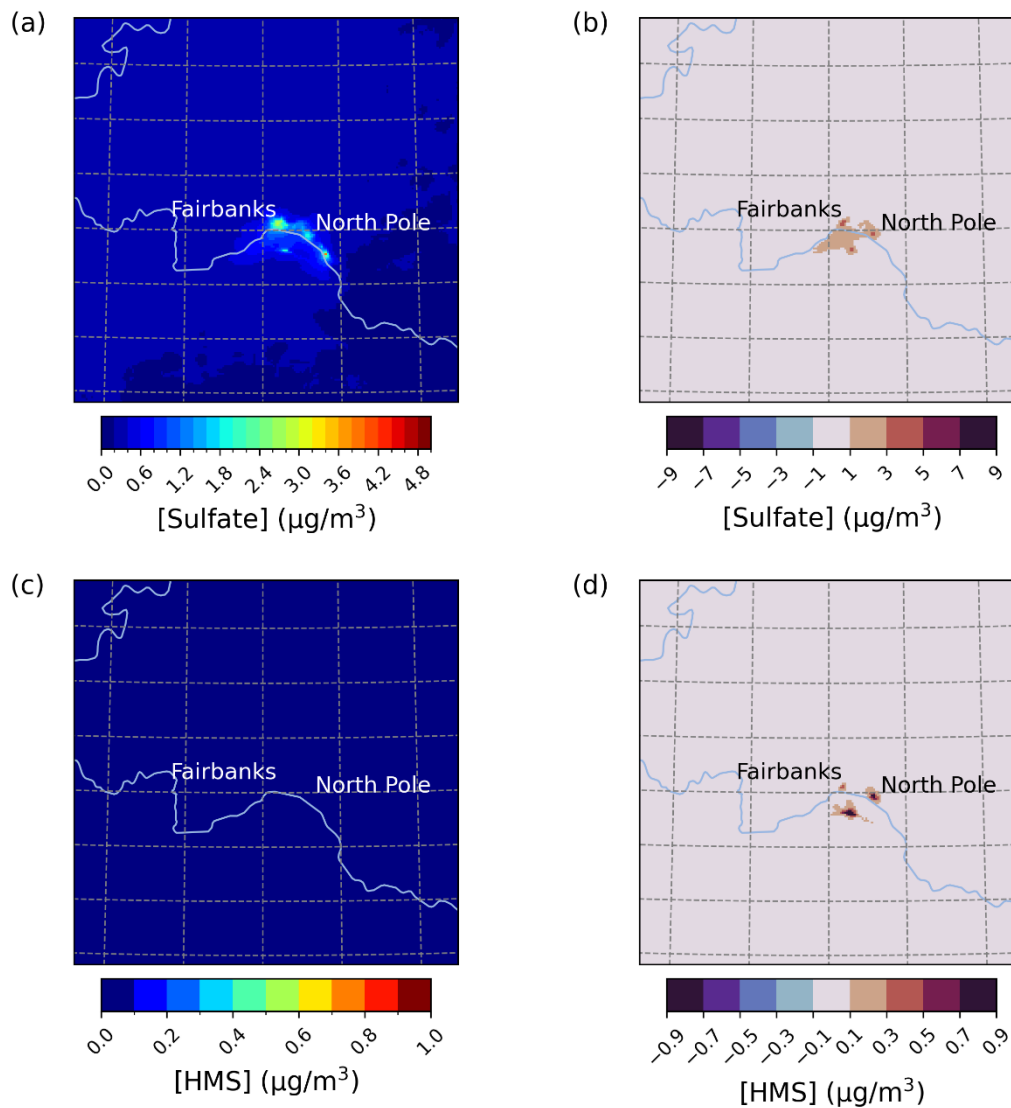
Figure 3. Episode average sulfate (a), and HMS (c) concentrations in the Base simulation along with daily max differences in sulfate (b), and HMS (d) concentrations between the Base_Het and Base CMAQ simulations over Fairbanks and North Pole AK for episode 2 (from November 4th, 2008, to November 17th, 2008). HMS formation was not included in Base CMAQ (i.e., HMS = 0 in the Base simulation). Domain size is 264.67 km by 264.67 km with a grid cell resolution of 1.33 km by 1.33 km.

In the Base_Het simulation of Episode 2, $PM_{2.5,sulf}$ was formed both in ALW and cloud liquid water (Fig. 4). Similar to Episode 1, the leading secondary formation pathway in downtown Fairbanks was the TMI-catalyzed O_2 pathway in both ALW and cloud water. This formation pathway split between the ALW and cloud formation pathways when modelled fog water content was around 0.025-0.05 g/m^3 for Nov. 5th and Nov. 7th, however, was completely overtaken by the cloud formation pathway on Nov. 15th when fog water content was > 0.175 g/m^3 (at both Fairbanks and North Pole), highlighting that when surface clouds, or fog water, is present, reactions in cloud water can compete with those in aerosol water. In North Pole, the leading ALW $PM_{2.5,sulf}$ formation pathway was also the TMI-catalyzed O_2 oxidation pathway with contributions from this pathway in cloud water as well. Sulfate formed via S(IV) oxidation by NO_2 in cloud water was slightly higher in North Pole than downtown Fairbanks for all cloud events even though NO_2 emissions are higher in downtown Fairbanks (Fig. S5). This could be due to higher cloud/fog pH in North Pole compared to downtown Fairbanks, as this pathway is known to favor pH > 5 (Clifton et al., 1988; Lee and Schwartz, 1983a; Littlejohn et al., 1993; Sarwar et al., 2013). HMS formation in ALW is also present in North Pole on the last day of Episode 2, corresponding with temperatures around -28 ºC and aerosol pH ~5.
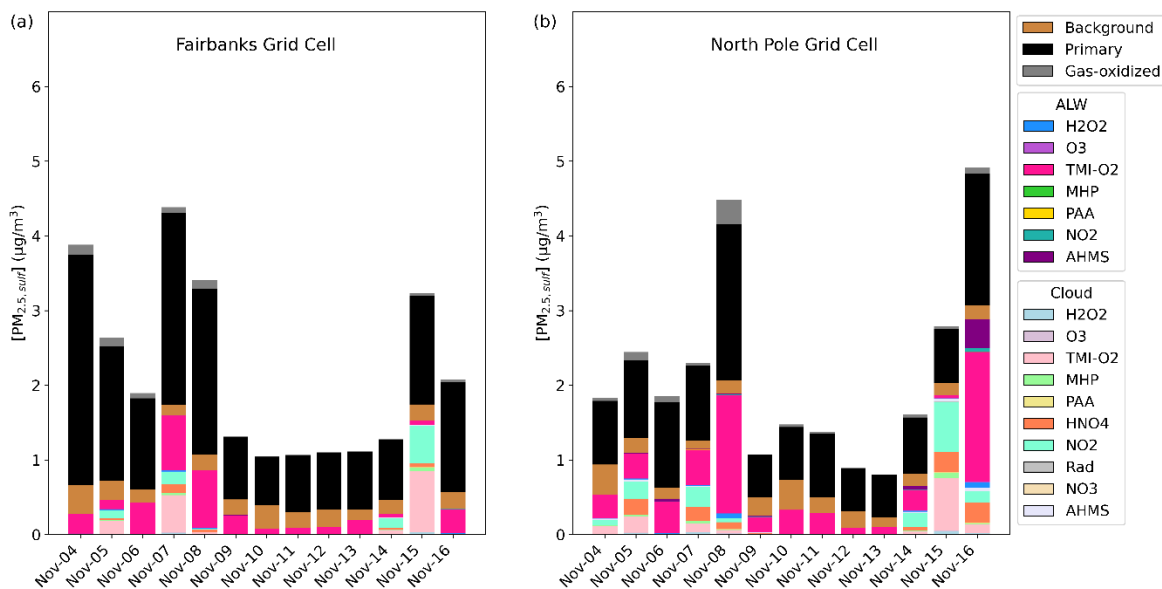
Figure 4. Particulate sulfur process/chemistry contributions and speciation (SO42- and HMS) in Downtown Fairbanks (a) located at the State Office Building (64.84 N, -147.72 W; grid cell 108,93) and North Pole (b) located at (64.76 N, -147.34 W; grid cell 122, 86) for episode 2 speciated by source and/or formation pathway. Secondary aqueous formation of PM2.5,sulf is broken out into two categories: ALW and Cloud, where ALW pathways represent the heterogeneous sulfur chemistry added in this study.

HMS contribution to $PM_{2.5,sulf}$ concentrations is further increased on Nov. 16th in North Pole in the TMI_sens model simulation (Fig. S7b). Despite this increase in HMS, total $PM_{2.5,sulf}$ predicted in this simulation is lower than in the Base_Het simulation for most of the episode. The compensation of the HMS formation pathway for the TMI-catalyzed O_2 formation pathway is not

as significant for this episode despite similar HCHO emissions (Fig. S5) and is likely due to higher temperatures (~ +15 °C warmer than E1).

3.1.3. Improved model performance for PM$_{2.5,sulf}$ in Fairbanks

Daily average PM$_{2.5,sulf}$ concentrations for the Base and Base_Het simulations were compared with 24-hour SO$_4^{2-}$ measurements taken every third day at the State Office Building in downtown Fairbanks (Fig. 5) (ADEC, 2023).
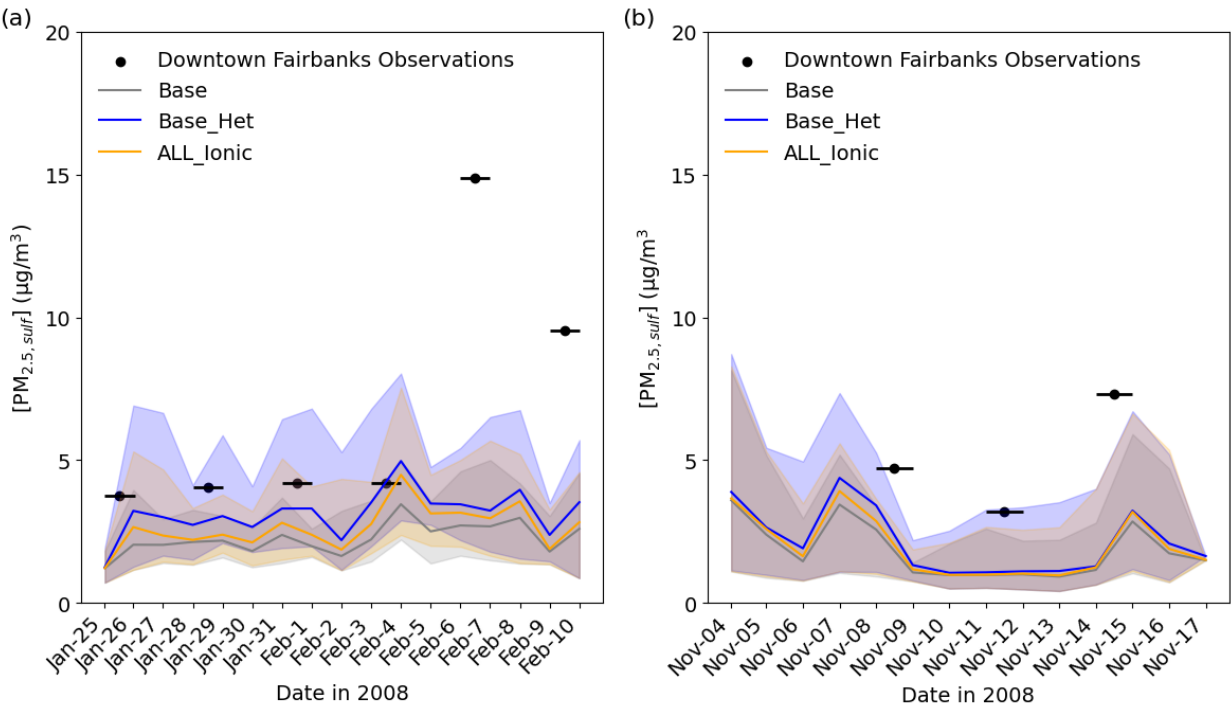

Figure 5. Timeseries comparing modelled PM$_{2.5,sulf}$ concentrations to measured SO$_4^{2-}$ concentrations at the State Office Building in Downtown Fairbanks (64.84 N, -147.72 W; grid cell 108,93) for episode 1 (a) and episode 2 (b). Lines represent daily average modelled values and shading represent hourly maximum and minimum concentrations for each day. Black lines represent the sampling period of the monitor measurements with black circles representing the mid-point of the 24-hour sampling period.

With the inclusion of heterogeneous sulfur chemistry in CMAQ (Base_Het), the mean bias in PM$_{2.5,sulf}$ improved by ~0.62 µg/m^3 during E1 and by ~0.36 µg/m^3 during E2 , reducing the model bias by up to ~1 µg/m^3 during E1 and up to ~ 0.85 µg/m^3 during E2. CMAQ still underpredicts PM$_{2.5,sulf}$ observations for both episodes, particularly during E1 for February 6th and 9th by ~11 and 7 µg/m^3 respectively. PM$_{2.5}$ speciation measurements during both episodes were only available for a single monitor located in Downtown Fairbanks, and therefore we were not able to assess model performance in North Pole, where modelled PM$_{2.5,sulf}$ concentrations can be higher by up to ~5-27 µg/m^3 (daily maximum difference) for E1 and ~2-2.4 µg/m^3 (daily

maximum difference) for E2. Although there were no measurements to compare with modelled North Pole results, higher $PM_{2.5,sulf}$ enhancements at North Pole are consistent with higher $PM_{2.5}$ concentrations at North Pole compared to Fairbanks (ADEC, 2017).

3.2 Modelled $PM_{2.5,sulf}$ formation enhancements over the Northern Hemisphere in Winter

455 To investigate model performance with the addition of heterogeneous sulfur chemistry for other locations and time periods that experience dark and cold conditions, Hemispheric CMAQ (HCMAQ) was run over the Northern Hemisphere from October 2015 to February 2016 (with the first two months as model spin up) for the same base and sensitivity simulations as above. $PM_{25,sulf}$ in China was of interest on this domain, given its haze events. High secondary and heterogeneously formed SO_4^{2-} and HMS have been documented to coincide with the high SO_2 emissions, high PM loadings, and high ALW during

460 Chinese haze events (Cheng et al., 2016; Elser et al., 2016; Li et al., 2017; Ma et al., 2020; Peng et al., 2021; Wang et al., 2016). Winter episode average modelled SO_2 over the northeast China and other parts of China can be > 20 ppb, episode average modelled $PM_{2.5}$ can be > 80 µg/m^3, and episode averaged ALW can be > 80 µg/m^3 in this region (Fig. S8).

Maximum enhancements in $PM_{2.5,sulf}$ for the Base_Het simulation occur largely in the North China Plain and northeast China

465 with some notable enhancement over India as well (Fig. 6) and led to a maximum daily increase in $PM_{2.5,sulf}$ by up to ~54 µgS/m^3 at a grid cell in southern China (27.1651 N, 107.5234 W; grid cell [149,67]) for this winter period (Fig. 6).
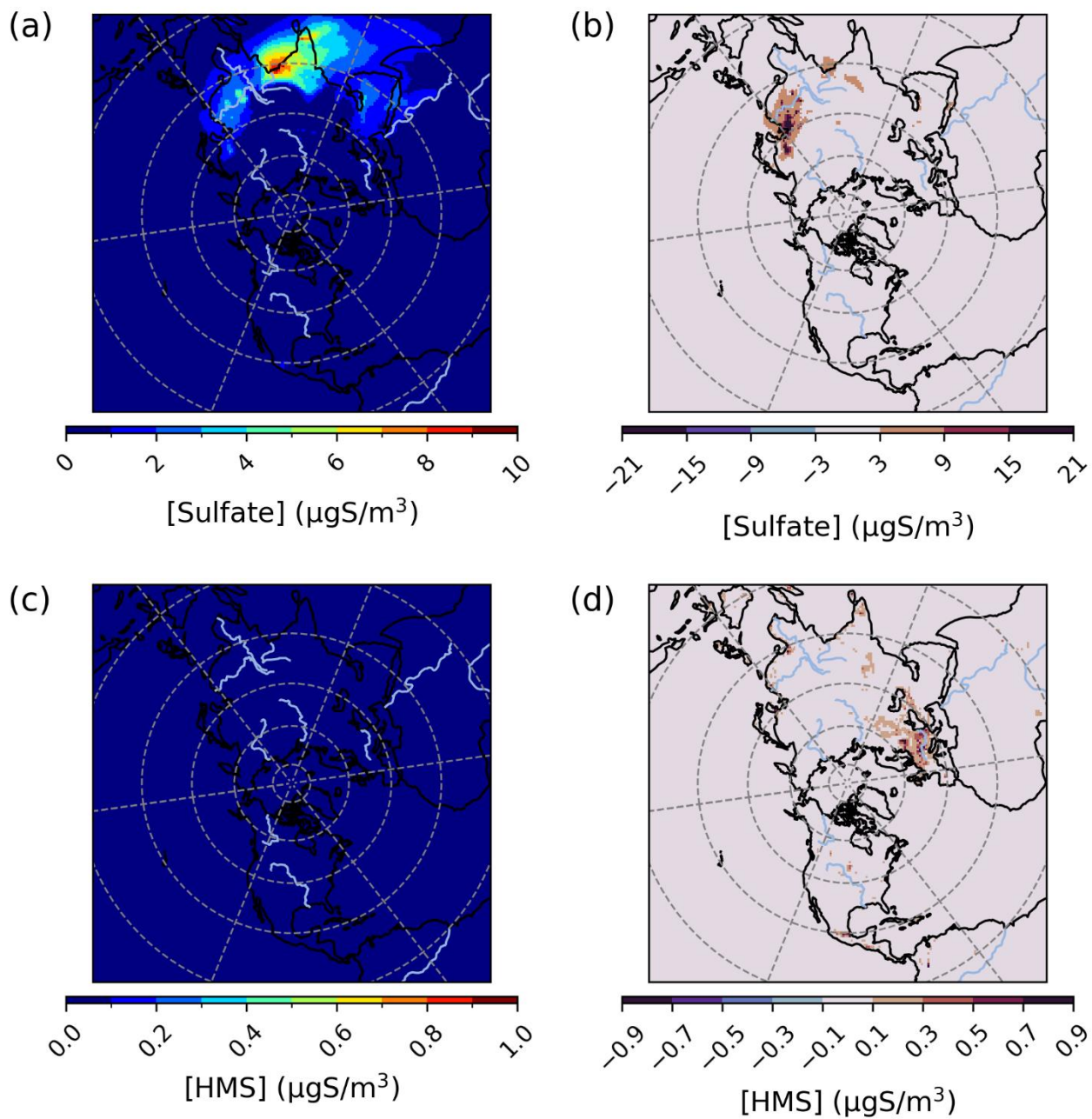
Figure 6. Episode average sulfate (a), and HMS (c) concentrations in the Base simulation along with maximum daily differences in sulfate (b), and HMS (d) concentrations between the Base_Het and Base CMAQ simulations over the Northern Hemisphere for a winter-time episode (from December 1st, 2015, to February 29th, 2016). HMS formation was not included in Base CMAQ. Differences are cast in micrograms of sulfur per meter cubed to be consistent with measurement units from EMEP.

This maximum daily enhancement is due almost entirely to an increase in predicted SO_4^{2-} (max daily concentration of 53

475    $\mu gS/m^3$ at this same location). On average SO_4^{2-} can increase by up to ~9 $\mu gS/m^3$ over a grid cell in northeastern China (45.6698 N, 127.9877 W; grid cell [122,64]). HMS contributions to $PM_{2.5,sulf}$ for the Base_Het run over this domain were less significant with a maximum daily concentration of ~2.6 $\mu gS/m^3$ in a grid cell near Tehran, Iran (36.7976 N, 51.6208 W; grid cell [137,119]).

480   For the TMI_sens simulation, maximum daily $PM_{2.5,sulf}$ concentrations increased from the Base simulation by up to ~33 $\mu gS/m^3$ and on average up to ~7 $\mu gS/m^3$ at a grid cell in Hebei, China (39.8603 N, 119.2348 W; grid cell [131,65]) (a reduced episodic enhancement in comparison to the Base_Het simulation). This maximum enhancement is also almost entirely attributed to SO_4^{2-} increases. HMS concentrations in the TMI_sens simulation, however, contributed up to ~2.8 $\mu gS/m^3$ (in maximum daily concentrations) in a grid cell in northeast China (45.6698 N, 127.9877 W; grid cell [122,64]) (Fig. S9). Predicted $PM_{2.5,sulf}$

485   concentrations in the TMI_NO2_sens and All_Ionic simulations were similar to the TMI_sens simulation for both predicted SO_4^{2-} and HMS concentrations with the exception of not reproducing as high of HMS concentrations in northeast China (Fig. S9).

The addition of heterogenous sulfur chemistry decreased the model bias during an extreme haze event on the HCMAQ domain

490   as well. Modelled $PM_{2.5,sulf}$ concentrations from a grid-cell over Beijing were compared to sulfate measurements at Tsinghua University in Beijing (Zhang et al., 2021b) (Fig. 7).
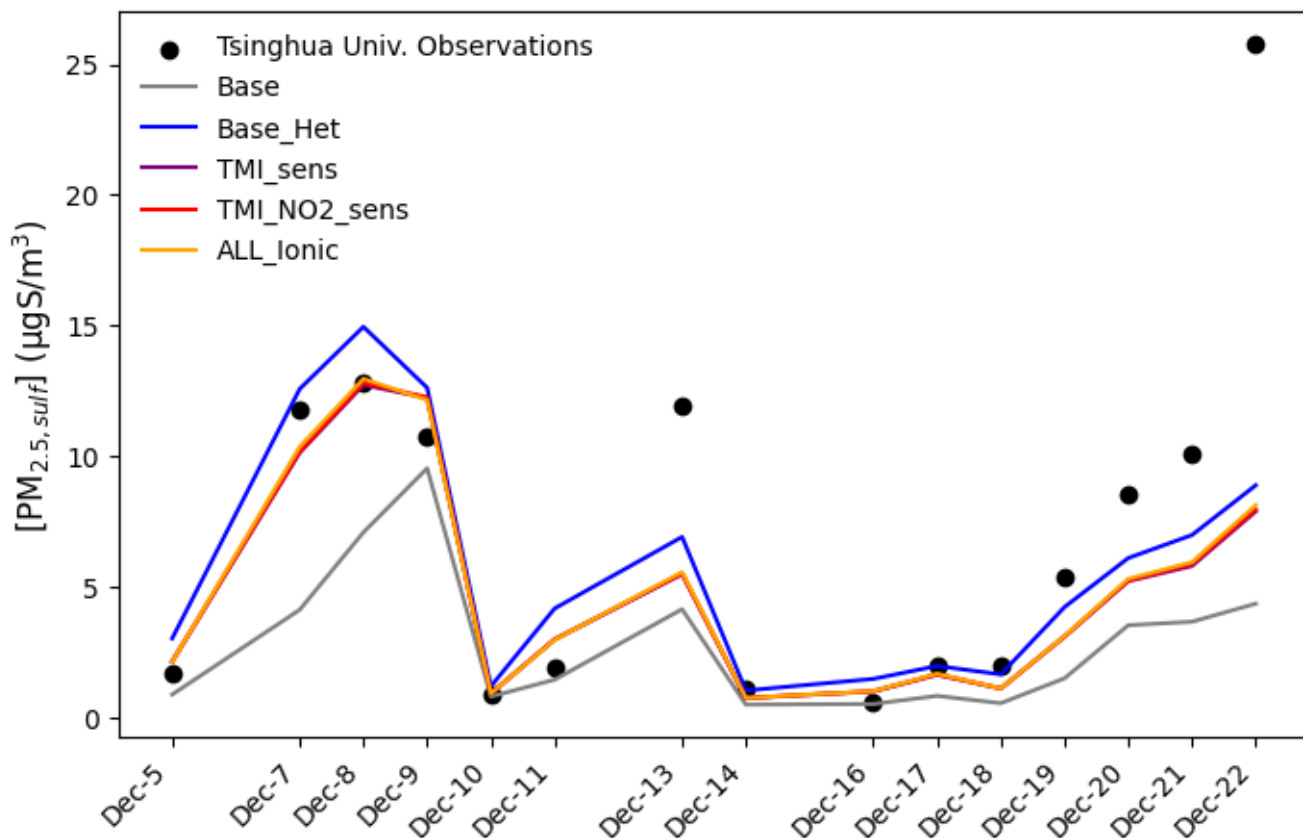
Figure 7. Model-measurement comparisons of PM$_{2.5,sulf}$ across all model runs for HCMAQ at a grid cell over Tsinghua University in Beijing, China from December 5th to December 22nd, 2015. Observations sourced from Zhang et al. (2021b)

The Base_Het and all additional sensitivity runs predicted higher PM$_{2.5,sulf}$ at this grid cell than the Base model simulation and reduced modelled mean bias by 2.9 µgS/m^3 (model mean bias with Base was -4.2 µgS/m^3 and mean bias with Base_Het was -1.3 µgS/m^3) (Fig. 7). Despite the overall improvement in model performance in the Base_Het simulation, a substantial gap in modeled and measured PM$_{2.5,sulf}$ still exists on Dec. 22nd. Daily averaged modeled SO$_2$, NO$_2$, HCHO and TMI concentrations (from Base HCMAQ, representing a lower-bound for SO$_2$ consumption) for this time period show that peak PM$_{2.5,sulf}$ concentrations coincide with the co-occurrence of heightened SO$_2$+TMI+NO$_2$ concentrations (Fig. S10). On Dec. 22nd, while SO$_2$ concentrations reach a daily average of ~22ppb, NO$_2$ and TMI concentrations are ~1/2 the concentrations they are Dec 7th-8th.

The enhancement in PM$_{2.5,sulf}$ is mainly attributed to SO$_4^{2-}$ increases, as HMS maximum daily concentrations over this grid cell for this time period were ~ 0.002 ugS/m^3 for Base_Het and the three sensitivity simulations. Simulated HMS for Base_Het and the sensitivities for the winter 2016 case were also ~0.002 ugS/m^3 (~0.006 ug/m^3). While the HCMAQ estimates may be

25

low, they are within the range of daily filter measurements of a polluted episode (from ~ 0 to 1.2 µg/m^3) reported in Ma et al. (2020).

Normalized mean biases (NMB) for PM$_{2.5,\text{sulf}}$ in the Base simulations over the N. Hemisphere ranged between -90% to 800% and NMB for the Base_Het simulation ranged from -90% to 980% (Fig. S11). The largest positive NMB occurred at a site in the Western U.S. for both simulations and is due, however, to very low modelled and observed concentrations. The mean biases at this location were only ~0.1-0.2 ugS/m^3 for both simulations, as this region was generally not affected by our updates (Fig. 6). Improvement of negative NMB occurred in the Base_Het run in some parts of the eastern U.S. and Canada, however caused and/or increased NMB in the positive direction in most of the eastern U.S. and Canada (Fig. S11). The change in NMB in Europe was not significant, despite enhancements from HMS formation. Regional aggregated model performance metrics can be found in Table S1.

3.3 CMAQ model performance changes over the Contiguous United States with the implementation of heterogeneous sulfur chemistry

CMAQ was run over the CONUS domain for both a winter and summertime episode to ensure that heterogeneous sulfur chemistry updates intended to be significant during dark and cold episodes had minimal impact on domains and episodes where this chemistry is less likely to dominate. For a January 2016 simulation over the CONUS domain PM$_{2.5,\text{sulf}}$ enhancements can be seen mainly over the eastern U.S. and western Canada (Fig. 8), on average were enhanced by up to ~ 1.5 µg/m^3. Average daily enhancements in Base_Het SO$_4^{2-}$ for the entire episode were up to ~1.5 µg/m^3 as well and daily average Base_Het HMS were up to ~0.7 µg/m^3.

PM$_{2.5,\text{sulf}}$ maximum daily enhancements for this episode, however, reached 28 µg/m^3 at a grid cell in southwestern Kansas (37.3983 N, -101.9184 W; grid cell [121,177]). It should be noted that total modelled daily averaged PM$_{2.5}$ concentrations at this grid cell was 575 µg/m^3 signifying a major PM event. PM$_{2.5,\text{sulf}}$ enhancements from SO$_4^{2-}$ at this grid cell and day contributed ~75% with HMS contributing ~ 25%. The leading PM$_{2.5,\text{sulf}}$ formation pathway at this grid cell, however, in the Base_Het run was the TMI-catalyzed O$_2$ oxidation pathway in ALW (Fig. S12). This pathway dominates at a few other locations (Fig. S12), however, gas-phase oxidation of SO$_2$ by OH is the leading secondary PM$_{2.5,\text{sulf}}$ formation pathway spatially, followed by cloud-aqueous oxidation by H$_2$O$_2$ and HNO$_4$.

The maximum daily average enhancement in HMS was ~ 13 µg/m^3 and occurred in the Ozarks in south central Missouri (36.6721 N, -92.9428 W; grid cell [114,243]) also coinciding with a major PM event (model daily average PM$_{2.5}$ concentrations of 301 µg/m^3) (Fig. 8).
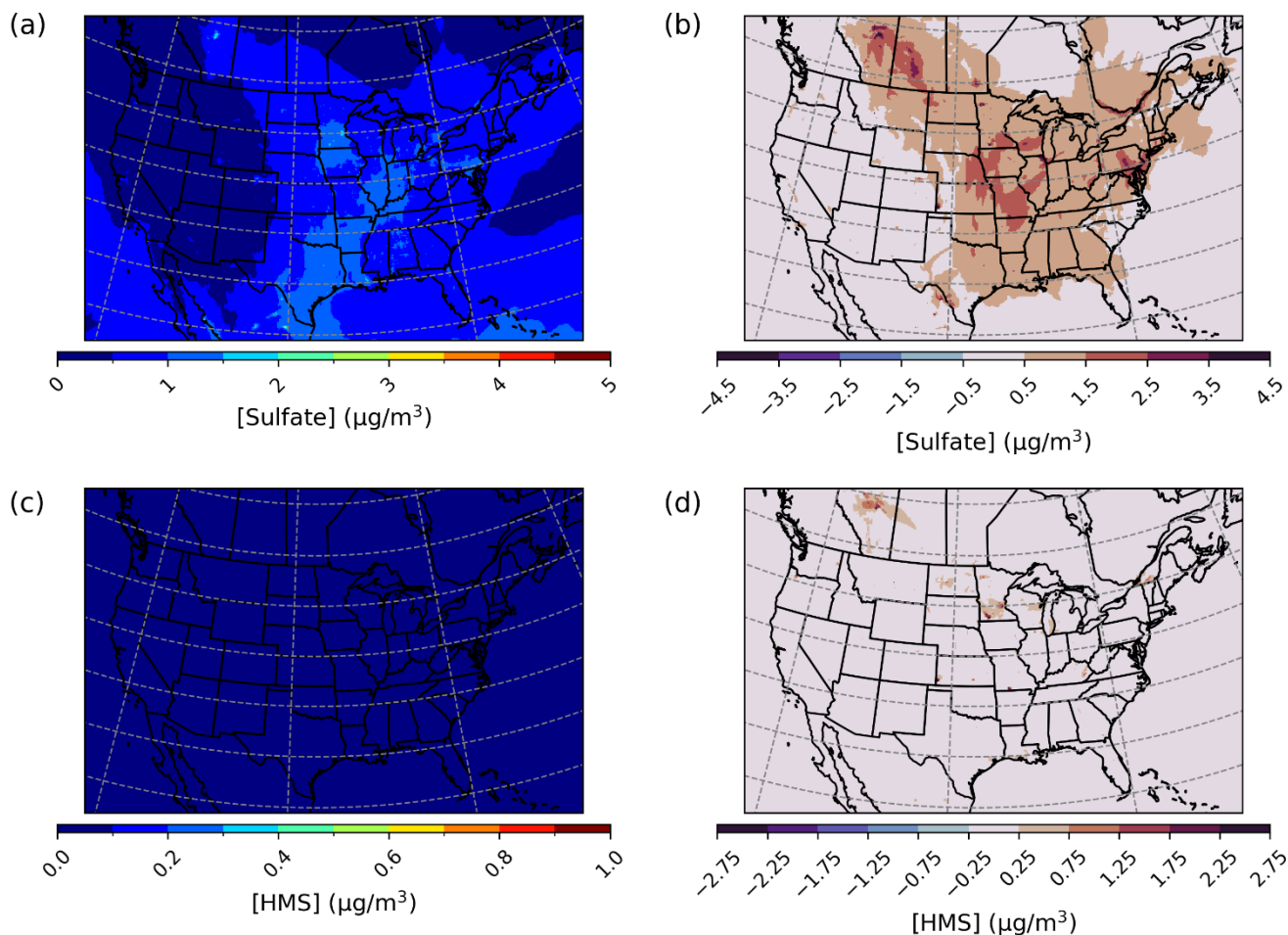
26

Figure 8. Episode average sulfate (a), and HMS (c) concentrations in the Base simulation along with maximum daily differences in sulfate (b), and HMS (d) concentrations between the Base_Het and Base CMAQ simulations over the Contiguous United States for a winter-time episode (January 2016). HMS formation was not included in Base CMAQ, and HMS mass concentrations are multiplied by the ratio of sulfate to HMS molecular mass.

550

$PM_{2.5,sulf}$ concentration enhancements in the TMI_sens simulation are similar to those in Base_Het with a lesser contribution from SO_4^{2-} production and a higher contribution from HMS production (Fig. S12 a and b). The highest maximum daily enhancement for the TMI_sens simulation occurred in the same grid cell in southwest Kansas discussed previously and was slightly lower than the Base_Het simulations maximum daily average enhancement (27.7 µg/m^3). The percentage of $PM_{2.5,sulf}$
555 that was SO_4^{2-} and HMS, however, was ~10% (3.2 µg/m^3) and ~90% (28.3 µg/m^3 or 24.5 µg/m^3-SO$_{4,eq}$). Other instances of HMS concentrations higher than 5 µg/m^3 for this run were infrequent and either coincided with major PM$_{2.5}$ events (PM$_{2.5}$

concentrations > 100 µg/m^3). The highest maximum daily enhancement in PM$_{2.5,sulf}$ for the TMI_NO2_sens and All_Ionic runs were 22 and 18 µg/m^3 respectively and occurred at the same grid cell in southwestern Kansas. Enhancements in PM$_{2.5,sulf}$ in this grid cell were mainly attributed to HMS for both the TMI_NO2_sens and All_Ionic simulations and were ~14-15 µg/m^3,

560 further demonstrating the importance of HMS to total PM$_{2.5,sulf}$ when a temperature and pH dependent TMI-catalyzed O$_2$ k_{chem} is used during a cold major PM event.

Both the Base and Base_Het CONUS simulations overestimate measurements in the western U.S. (Fig. 9) with the highest positive NMB ~450% in Washington state with little difference in the NMB between the two runs – as this region was generally

565 not affected by the implementation of heterogeneous sulfur chemistry (Fig. 8). It should also be noted that mean bias in the western U.S. is fairly low (Fig. S13), and therefore the high NMB in this region is a result of overall low PM$_{2.5,sulf}$ concentrations (both modelled and measured). Negative NMB of PM$_{2.5,sulf}$ in the eastern U.S. in the Base run are ameliorated in the Base_Het runs, particularly in the Ohio River Valley and southeast U.S.; however, areas in the east with good model PM$_{2.5,sulf}$ performance in the Base run were mostly overpredicted in the Base_Het run. Model performance differences across

570 the additional sensitivity runs were minimal however all sensitivity runs had a lower positive NMB at the AQS sites around Chicago compared to the Base_Het (Fig. S14), and the TMI_sens simulation had the lowest positive NMB and mean bias at the AQS site in south central Missouri out of all of the newly implemented model runs.
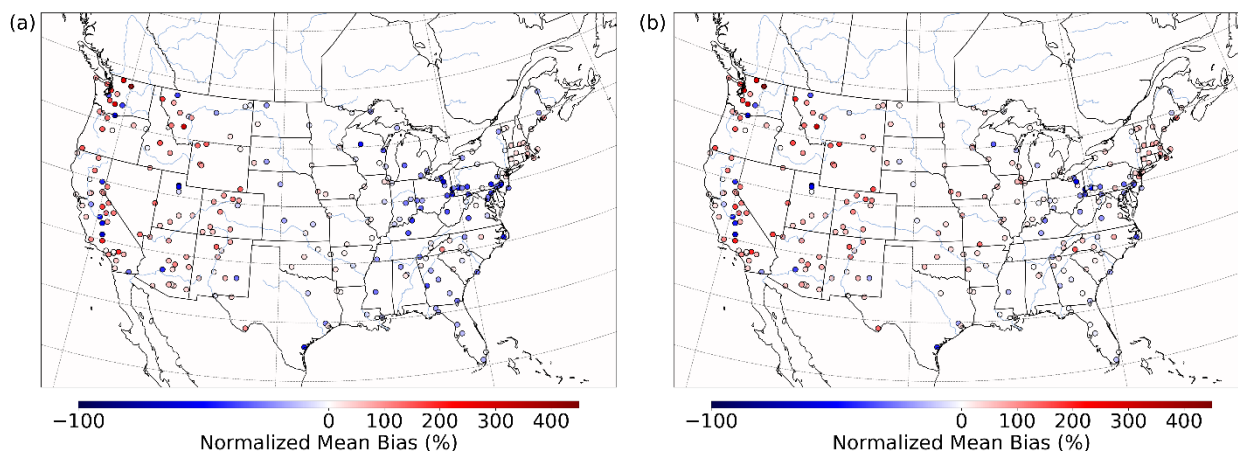

575 **Figure 9. Normalized Mean Bias in PM2.5,sulf concentrations by monitor over the CONUS domain for a winter-time episode (January 2016) for Base CMAQ (a) and Base_Het CMAQ (b).**

For a July 2016 simulated episode over the CONUS domain, overall daily enhancements in Base_Het PM$_{2.5,sulf}$ were on average 0.05 µg/m^3 across the entire domain. Daily SO$_4^{2-}$ enhancements were more prevalent spatially over the eastern part of the U.S.,

580 particularly in the South and Ohio River Valley (Fig. 10), and HMS formation was more prevalent in the western part of the domain.

28

Maximum daily PM$_{2.5,\text{sulf}}$ enhancements in the Base_Het model run reached up to 789 µg/m^3, at a grid cell in Monterey County, California (36.2839 N, -121.9208 W; grid cell [135,30]) on July 26th largely due to high daily averaged HMS concentrations (~533 µg/m^3) (Figure 10) and coincide with the Soberanes fire at this location in late July (Queally, 2016). SO$_4^{2-}$ concentration
585 enhancements were also significant at this grid cell (~255 µg/m^3). It should be noted that modelled daily averaged PM$_{2.5}$ and HCHO concentrations for this day and grid cell were also extremely high (9389 µg/m^3 and 577ppbV respectively).
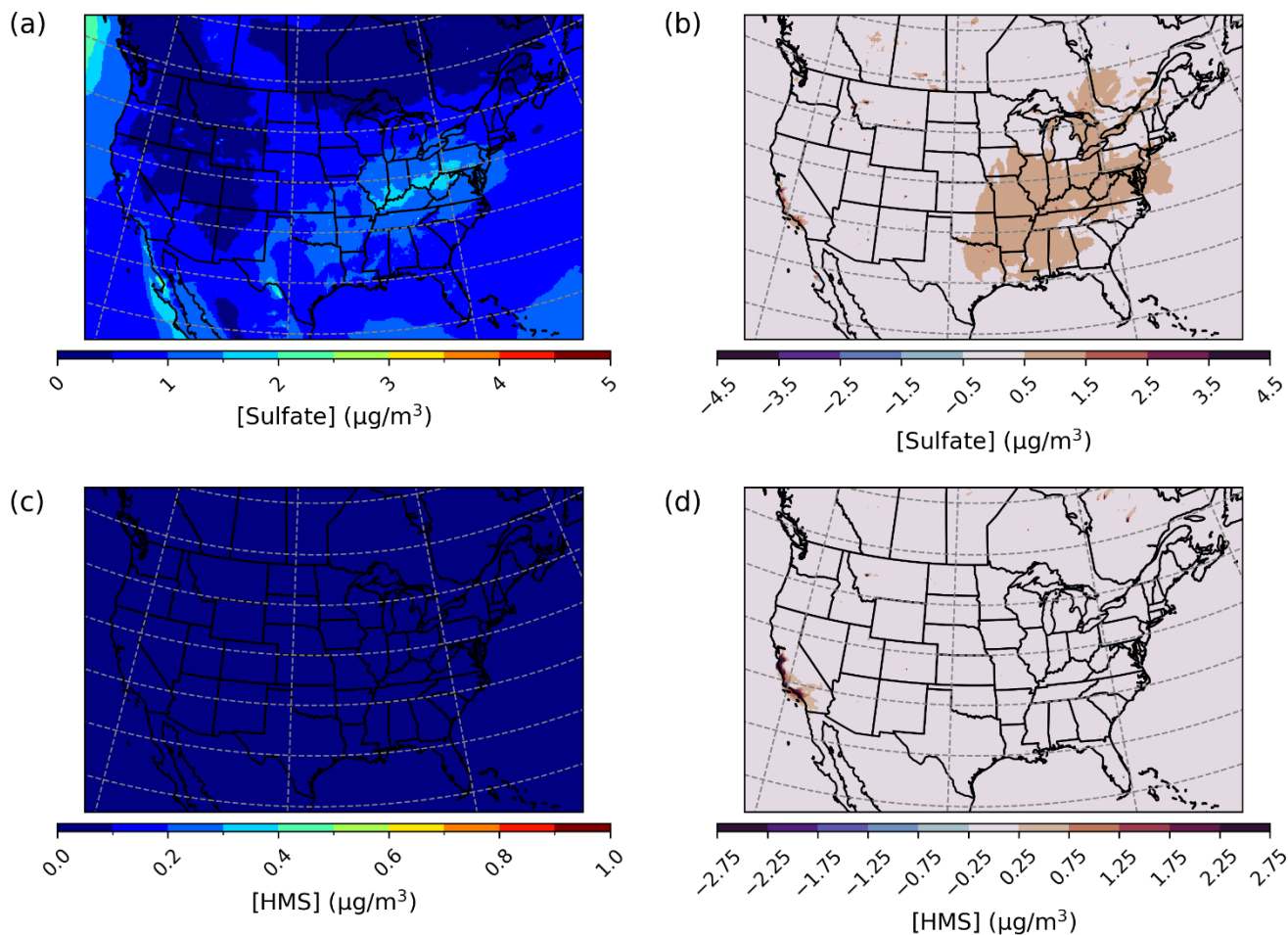

Figure 10. Episode average sulfate (a), and HMS (c) concentrations in the Base simulation along with maximum daily differences in
590 **sulfate (b), and HMS (d) concentrations between the Base_Het and Base CMAQ simulations over the Contiguous United States for a summer-time episode (July 2016). HMS formation was not included in Base CMAQ, and HMS mass concentrations are multiplied by the ratio of sulfate to HMS molecular mass.**

In the same grid cell and time where there were maximum daily enhancements in PM$_{2.5,\text{sulf}}$ in the Base_Het run occur, TMI_sens simulated PM$_{2.5,\text{sulf}}$ increased by ~791 µg/m^3 with HMS contributing ~732 µg/m^3. Similar to results in other domains and
595 episodes, in the TMI_sens simulation, HMS formation is higher and SO$_4^{2-}$ enhancement decreases in comparison to the

29

Base_Het. Average daily SO_4^{2-} enhancements in the TMI_sens reached up to 4 µg/m³ and in the Base_Het reached up to 11 µg/m³, and both occurred in the same grid cell in Monterey, California mentioned before. For the TMI_NO2_sens simulation, maximum daily enhancement in $PM_{2.5,sulf}$ concentrations are similar to the TMI_sens (~791 µg/m³) with a slightly lower contribution from HMS (~720 µg/m³). Maximum daily $PM_{2.5,sulf}$ enhancements were the lowest in the All_Ionic model run, however still a substantial enhancement (~788 µg/m³; occurring in the same grid cell and time as all other models run maximum daily enhancements) with HMS contributing ~709 µg/m³ and SO_4^{2-} contributing ~ 79 µg/m³ to this enhancement. Spatial distribution of SO_4^{2-} enhancements for all sensitivity runs were similar to the Base_Het SO_4^{2-} enhancements (Fig. S15).

Both the Base and Base_het simulations mainly overestimate $PM_{2.5,sulf}$ concentrations in the northwest U.S. and have similar performance (Fig. 11 and Fig. S16) due to this region not generally being affected by heterogeneous sulfur chemistry updates (with the exception of a few locations that aren't in the same grid cells as an AQS monitor). Although there were significant enhancements in HMS and off the Californian coast, HMS concentrations greater than 5 ug/m³ were limited to a few grid cells on July 26th (when maximum concentrations of HMS were predicted) and did not reach the nearest AQS monitors. Higher daily HMS concentrations were predicted south of Monterey down the California Coast the following 2 days (which did not have a corresponding AQS measurement). Increased SO_4^{2-} formation in the Base_Het simulation improved modelled underestimates in some parts of the Eastern U.S. (Fig. 11 and Fig. S16), particularly in parts of the southeast (Fig. S17).
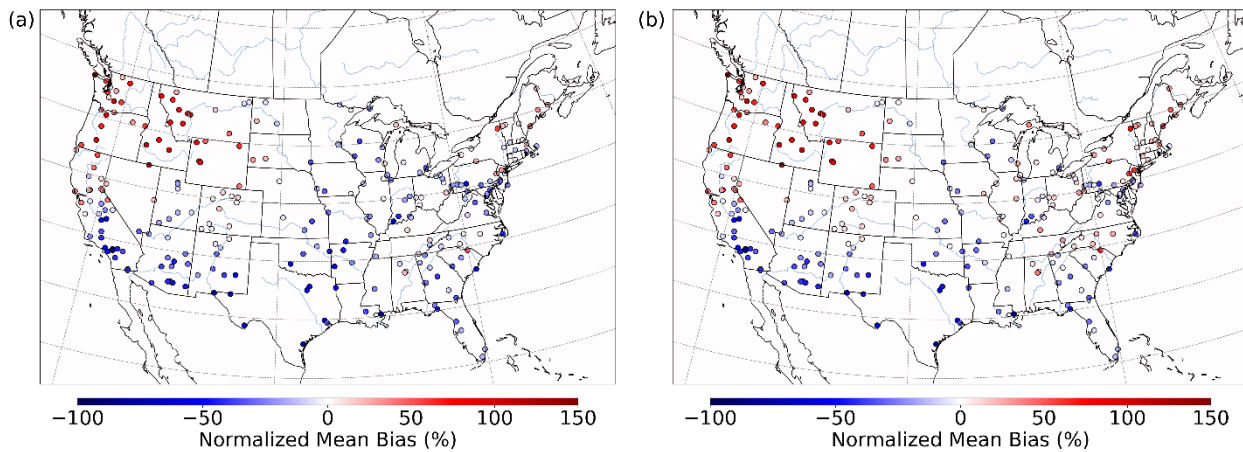

Figure 11. Normalized Mean Bias in PM2.5,sulf concentrations by monitor over the CONUS domain for a summer-time episode (July 2016) for Base CMAQ (a) and Base_Het CMAQ (b).

Although the implementation of heterogeneous sulfur chemistry generally led to minimal enhancements in both SO_4^{2-} and HMS over the entire CONUS domain for both episodes, it did slightly increase SO_4^{2-} in the eastern U.S. and substantially increased HMS concentrations during major PM events, including but not limited to wildfires. Enhancements in SO_4^{2-} could potentially impact the formation of secondary organic aerosol (Fan et al., 2022). SO_4^{2-} is an important nucleophile in the

620 formation of isoprene-epoxydiol (IEPOX)-derived organosulfates (Surratt et al., 2010) and enhancements in SO_4^{2-} concentration may help reduce model underpredictions for IEPOX organosulfates (Budisulistiorini et al., 2017). Aqueous SO_4^{2-} in the presence of Fe^{3+} and other isoprene-derived SOA precursors has been shown to enhance the production of C2-C4 organosulfur compounds as well (Huang et al., 2019). Modelled enhancements in both SO_4^{2-} and HMS during wildfires are both particularly high due to extraordinarily high emissions during these events in general. The TMI_sens predicted the highest

625 HMS concentrations across all model simulations, however max daily SO_4^{2-} concentrations in the TMI_NO2_sens were higher in comparison to the TMI_sens, indicating the importance of the heterogeneous NO_2 oxidation pathway during wildfire events. Wildfires release high concentrations of black carbon which can inhibit modelled photolysis of NO_2, and high in-plume oxidant concentrations can facilitate it's regeneration (Buysse et al., 2019; Xing et al., 2017).

4 Discussion

630 4.1 Improved model performance with heterogeneous sulfur chemistry in dark cold episodes

Traditional mechanisms of secondary sulfate formation have not been able to reproduce high observed sulfate concentrations experienced during Fairbanks and North Pole, AK winters. The added heterogeneous sulfur chemistry in ALW in this study enhanced modelled wintertime $PM_{2.5,sulf}$ concentrations in this domain as well as in China, where high wintertime $PM_{2.5,sulf}$ concentrations have also been observed (ADEC, 2017; Cheng et al., 2016; Ma et al., 2020; Moch et al., 2018; Wang et al.,

635 2016; Zhang et al., 2021b). Inclusion of these reactions improved model performance in these regions (Fig. 5 and Fig. 7). $PM_{2.5,sulf}$ enhancements between the Base and Base_Het simulations during a PM episode (E1) in the Fairbanks domain showed that heterogeneous sulfur chemistry in ALW can increase daily $PM_{2.5,sulf}$ concentrations by up to 11 µg/m^3 across the entire domain for this dark and cold modeling episode (Fig. 2). At grid cells in downtown Fairbanks and North Pole, maximum daily enhancements in $PM_{2.5,sulf}$ during E1 can range ~1-1.5 µg/m^3 and ~ 4-25 µg/m^3 respectively (Fig. 2 and S3), across all of the

640 heterogeneous sulfur chemistry configurations tested in this work. In this same domain during E2, modelled secondary $PM_{2.5,sulf}$ formation takes place primarily via in-cloud formation pathways (Fig. 4 and S7), highlighting the enduring importance of cloud-aqueous chemistry in modeling $PM_{2.5,sulf}$ formation when substantial liquid cloud water is present.

$PM_{2.5,sulf}$ enhancements from heterogeneous sulfur chemistry for the wintertime HCMAQ simulations occurred mostly in

645 China, South Asia and Europe (Fig. 6). Maximum daily enhancements in $PM_{2.5,sulf}$ ranged between 33-54 µgS/m^3 across heterogeneous sulfur chemistry configurations tested in this work and were all located in China. Heterogeneous sulfur chemistry updates also improved negative model bias for $PM_{2.5,sulf}$ in Canada (Table S1) where wintertime temperatures can be extremely cold and residential home heating along with industrial emissions may be high (Cho et al., 2009; Liggio et al., 2016; Stroud, 2009).

650

In general, there were minimal changes in predicted $PM_{2.5,sulf}$ in regions and during episodes that do not experience extreme cold and dark conditions. Positive model bias in estimating $PM_{2.5,sulf}$ in Europe for the HCMAQ simulation, slightly increases in the Base_Het, TMI_sens, and TMI_NO2_sens simulations, however, remains unchanged in the All_Ionic simulation. Similarly, model bias in estimating $PM_{2.5,sulf}$ in the U.S. for the HCMAQ also increases slightly from the Base in all the newly implemented model runs by 0.05 $\mu g/m^3$ (Table S1).

The inclusion of heterogeneous sulfur chemistry had a lesser impact on modelled $PM_{2.5,sulf}$ over the CONUS domain (in comparison to the Fairbanks and HCMAQ domains) with the exception of high PM events. Interestingly, the inclusion of these missing pathways reduced some of the negative bias in $PM_{2.5,sulf}$ concentrations in the Southeast during warm and light summertime conditions (Fig. 11, S16, and S17) and are mostly from SO_4^{2-} enhancements (Fig. 10 and S15). SO_4^{2-} can participate as a reactant and a modulator of pH in the heterogeneous formation of IEPOX derived organosulfates (Marais et al., 2016; Pye et al., 2017; Pye et al., 2020) and improved SO_4^{2-} negative bias may also improve model performance of IEPOX-SOA.

4.2 Contribution of HMS to $PM_{2.5,sulf}$

In this study we found that HMS, a previously un-tracked aerosol species in CMAQ, can contribute substantially to total $PM_{2.5,sulf}$ dependent on HCHO and SO_2 concentrations, temperature, and heterogeneous sulfur chemical kinetics chosen. During E1 in Fairbanks, HMS concentrations in North Pole are higher in comparison to Fairbanks. Given stagnant conditions for this domain and episode, emissions tend to stay local (ADEC, 2017; Gaudet, 2012; Tran, 2011) . Thus, HCHO from residential wood combustion and SO_2 from home heating oil in North Pole, a largely residential area, compared to downtown Fairbanks, are the likely dominating reasons for higher HMS concentrations when comparing the two areas.

Modelled HMS generally had a lesser impact on both the N. Hemispheric and CONUS domains (generally contributing < 1 ug/m3), with a few anomalous exceptions. Modelled HMS in HCMAQ runs primarily appeared in Europe and China, where wintertime HMS has previously been predicted (Moch et al., 2020). On the CONUS domain, HMS concentrations were predicted to by high during major PM events (including but not limited to wildfires) which illuminates the importance of HMS during high atmospheric loadings of both SO_2 and HCHO.

Across all modelled domains and episodes, the TMI_sens model run predicted the highest HMS concentrations and may represent an upper bound on modelled HMS concentrations. Ultimately, more resolved measurements of speciated $PM_{2.5}$ that can separate out HMS and SO_4^{2-} (Campbell et al., 2022) can help discern their relative contributions to $PM_{2.5,sulf}$ mass and help constrain future modelled heterogeneous sulfur chemical kinetics.

4.3 $PM_{2.5,sulf}$ formation pathways of interest during cold and dark episodes

In addition to the inclusion of both heterogeneous SO_4^{2-} and HMS formation in CMAQ, we determined which $PM_{2.5,sulf}$ formation pathways are the most important given ionic strength, pH, and temperature regimes characteristic of dark and cold

685 conditions. Across both the Fairbanks and CONUS domains in the Base_Het during the wintertime, the most prevailing heterogeneous SO_4^{2-} formation pathway was the TMI-catalyzed O_2 pathway (Fig. 2, 4, S12). In the TMI_sens E1 in Fairbanks, however, this formation pathway was the third most important behind HMS formation and the NO_2 pathway (Fig. S3). Although the modelled pH for the TMI_sens ranged between 3-6 for Fairbanks and North Pole and for both episodes (Fig. S4) which included the optimal pH for this pathway (pH=4.2; (Ibusuki and Takeuchi, 1987)), the dampening of this pathway can

690 also be attributed to the extremely cold temperatures (modelled average -30° C or 243° K).

TMI_sens modelled aerosol pH was seen to be least acidic in comparison to all of the other model simulations, especially in North Pole (Fig. S4). As noted before, HMS was the largest contributor to secondary $PM_{2.5,sulf}$ formation at North Pole, the formation (and loss) rates of which increase with increasing pH (Ervens et al., 2003; Kok et al., 1986) (Fig. 2). Aerosol pH

695 and ALW calculations in ISORROPIA II only consider inorganic species. Organic species (e.g., organic acids) may also increase aerosol acidity (Zuend et al., 2011; Zuend and Seinfeld, 2012), and therefore the predicted aerosol pH in the TMI_sens might represent an overprediction. Aerosol pH for the Base_Het, TMI_NO2_sens, and All_Ionic model simulations were similar at both North Pole and Fairbanks with both sensitivity simulations predicting slightly higher pH than the Base_Het simulation during E1 and slightly lower pH during E2.

700

The impacts of increased ionic strength were explored with respect to the NO_2, O_3, and H_2O_2 oxidation pathways (note that ionic strength inhibition of the TMI-O_2 pathway is included in the Base_Het simulations as well). Ionic strength impacts added to the NO_2 pathway (in the TMI_NO2_sens) had the highest impact on the formation of SO_4^{2-} via this pathway (Fig. S3 and S7 c and d) in the Fairbanks domain for both episodes. Although the ionic strength for this pathway was bounded at 1.14 M,

705 an increase in aerosol ionic strength from 0.1 M to the upper bound of 1.14 M increased the k_{chem} for this pathway by ~2 orders of magnitude (Chen et al., 2019). Ionic strength impacts on the H_2O_2, and O_3 heterogeneous sulfur oxidation pathways had minimal impact during the wintertime PM episodes in Fairbanks and North Pole, only accounting for $\leq$~0.2 $\mu g/m^3$ in the All_Ionic model simulation (Fig. S3 and Fig. S7). These particular pathways were not assumed to be prolific given the lack of photochemistry during this episode; however with an ionic strength change from 0 to 5 M, the 3rd-order aqueous-phase rate

710 coefficient for the H_2O_2 heterogeneous sulfur pathway can increase by more than 40% regardless of pH or temperature (Maaß et al., 1999; Millero et al., 1989). The ionic strength used to calculate the ionic strength effect factor for this k_{chem} was limited to a maximum of 5 M; however recent studies have observed significant ionic-strength enhancement up to 14 M (Liu et al., 2020). For SO_4^{2-} formation via heterogeneous oxidation by O_3, the k_{chem} for this pathway can increase by ~80% with an ionic

strength increase from 0.1 to 0.8 M (Lagrange et al., 1994; Song et al., 2021b) at temperatures characteristic of Fairbanks winters, however these effects were not seen due to the lack of ozone modelled given the dark and cold conditions.

5 Conclusion

Air quality modelling of secondary sulfate has traditionally only included in-cloud aqueous- and gas-phase SO_2 oxidation pathways, often resulting in underpredictions of observed $PM_{2.5,sulf}$, especially during the cold and polluted conditions characteristic of wintertime PM and haze events (ADEC, 2017; Gao et al., 2016). In this study we implemented heterogeneous sulfur chemistry in aerosol liquid water in CMAQ to resolve model-measurement gaps in $PM_{2.5,sulf}$ concentrations during extreme wintertime PM episodes in and around Fairbanks, Alaska. We compared modelled $PM_{2.5,sulf}$ (SO_4^{2-}+HMS) concentrations to sulfate measurements at several measurement sites (under the assumption that HMS may be included in the sulfate observations (Dovrou et al., 2019)). Negative model bias improved in Fairbanks during winter and fall with these updates and also improved in Beijing, another location known to experience wintertime haze events. When applied more broadly to larger domains and other seasons, the update also resolved underestimations of $PM_{2.5,sulf}$ concentrations both in the United States and globally, however mostly did not have a huge impact when over domains that were not as dark and cold. HMS was found to be an important contributor to $PM_{2.5,sulf}$ mass during dark and cold episodes, however, to better understand the ratio of sulfate to HMS, more observations of HMS are necessary. Recently, the Alaskan Layered Pollution And Chemical Analysis (ALPACA) field campaign (Simpson et al., 2024) was conducted in and around Fairbanks during January-February 2022 and will offer observations to elucidate important sulfate and HMS formation pathways in the area and better characterize source apportionment of $PM_{2.5,sulf}$. Ultimately, HMS and sulfate formed via the TMI-catalysed O_2 and NO_2 pathways proved to be the most important to $PM_{2.5,sulf}$ formation pathways in Fairbanks and North Pole and require further investigation in the context of $PM_{2.5,sulf}$ control strategies. Finally, while this study aims to include ionic strength, pH, and temperature impacts on $PM_{2.5,sulf}$ formation in CMAQ, the ionic strength, pH and temperature ranges under which Henry's law, reaction rates, and other coefficients and parameters were derived experimentally and may not be representative of concentrated aerosol water or the extreme environment of subarctic and arctic wintertime conditions. Laboratory studies are needed to extend the bounds of these parameters and determine rate expressions appropriate for the concentrated conditions characteristic of aerosol water.

Disclaimer: The views expressed in this article are those of the authors and do not necessarily represent the views or policies of the US Environmental Protection Agency, Alaska Department of Environmental Conservation, or the University of North Carolina at Chapel Hill.

Author Contributions: HOTP, KF, SG and NB were responsible for conceptualization and funding acquisition. RG was responsible for meteorology development and prepared meteorology inputs. GP was responsible for emissions development and prepared emissions inputs. SF, KF and HOTP were involved with the methodology. SF and KF were involved with the

software. KF lead the model validation. SF, KF and DH were involved in the investigation and SF and KF lead the formal analysis. SF, KF, and DH were responsible for data curation. KF and HOTP were both involved with supervision and project administration. SF, KF, RG and GP were involved in writing the original draft. All co-authors contributed to writing-review and editing.

750

Code availability: CMAQ is available at https://github.com/USEPA/CMAQ and CMAQv5.3.2 is archived at https://doi.org/10.5281/zenodo.4081737 (U.S.EPA, Office of Research and Development, 2020). The exact CMAQ code and data used in this work will be available at https://catalog.data.gov/dataset/data-for-predicted-impacts-of-heterogeneous-
765 chemical-pathways-on-particulate-sulfur-over-f.

References

ADEC. (2014). *Alaska Air Quality Control Plan*. Retrieved from Juneau, AK: https://dec.alaska.gov/media/6987/iii-d-5-06-emission-inventory-adopted-122414.pdf
ADEC. (2017). *Amendments to: State Air Quality Control Plan. Section III. Area-wide Pollutant Control Program; D.*
770 *Particulate Matter; 5. Fairbanks North Star Borough PM2.5 Control Plan*. Retrieved from https://dec.alaska.gov/air/anpms/communities/fbks-pm2-5-moderate-sip/
ADEC. (2019). *Amendments to: State Air Quality Control Plan. Vol. II: III.D.7.3 Non-Attainment Area Boundary and Design Episode Selection. Public Notice Draft*. Retrieved from https://dec.alaska.gov/air/anpms/communities/fbks-pm2-5-public-notice-version-serious-sip/
775 ADEC. (2023). *Annual Air Quality Monitoring Network Plan*. Retrieved from Anchorage, Alaska: https://dec.alaska.gov/air/air-monitoring/monitoring-plans/#nogo
Alexander, B., Park, R. J., Jacob, D. J., and Gong, S. (2009). Transition metal-catalyzed oxidation of atmospheric sulfur: Global implications for the sulfur budget. *Journal of Geophysical Research: Atmospheres, 114*(D2). doi:https://doi.org/10.1029/2008JD010486
780 Ali, H. M., Iedema, M., Yu, X. Y., and Cowin, J. P. (2014). Ionic strength dependence of the oxidation of SO2 by H2O2 in sodium chloride particles. *Atmospheric Environment, 89*, 731-738. doi:https://doi.org/10.1016/j.atmosenv.2014.02.045

Altwicker, E. R., and Nass, K. K. (1983). Evidence for enhanced mass transfer and synergistic catalysis of aqueous phase sulfur dioxide oxidation by mixtures of manganese and iron. *Atmospheric Environment (1967), 17*(1), 187-190. doi:https://doi.org/10.1016/0004-6981(83)90024-0

Appel, K. W., Bash, J. O., Fahey, K. M., Foley, K. M., Gilliam, R. C., Hogrefe, C., Hutzell, W. T., Kang, D., Mathur, R., Murphy, B. N., Napelenok, S. L., Nolte, C. G., Pleim, J. E., Pouliot, G. A., Pye, H. O. T., Ran, L., Roselle, S. J., Sarwar, G., Schwede, D. B., Sidi, F. I., Spero, T. L., and Wong, D. C. (2021). The Community Multiscale Air Quality (CMAQ) model versions 5.3 and 5.3.1: system updates and evaluation. *Geosci. Model Dev., 14*(5), 2867-2897. doi:10.5194/gmd-14-2867-2021

Appel, K. W., Napelenok, S. L., Foley, K. M., Pye, H. O. T., Hogrefe, C., Luecken, D. J., Bash, J. O., Roselle, S. J., Pleim, J. E., Foroutan, H., Hutzell, W. T., Pouliot, G. A., Sarwar, G., Fahey, K. M., Gantt, B., Gilliam, R. C., Heath, N. K., Kang, D., Mathur, R., Schwede, D. B., Spero, T. L., Wong, D. C., and Young, J. O. (2017). Description and evaluation of the Community Multiscale Air Quality (CMAQ) modeling system version 5.1. *Geosci. Model Dev., 10*(4), 1703-1732. doi:10.5194/gmd-10-1703-2017

Boyce, S. D., and Hoffmann, M. R. (1984). Kinetics and mechanism of the formation of hydroxymethanesulfonic acid at low pH. *The Journal of Physical Chemistry, 88*(20), 4740-4746. doi:10.1021/j150664a059

Brüggemann, M., Xu, R., Tilgner, A., Kwong, K. C., Mutzel, A., Poon, H. Y., Otto, T., Schaefer, T., Poulain, L., Chan, M. N., and Herrmann, H. (2020). Organosulfates in Ambient Aerosol: State of Knowledge and Future Research Directions on Formation, Abundance, Fate, and Importance. *Environmental Science & Technology, 54*(7), 3767-3782. doi:10.1021/acs.est.9b06751

Budisulistiorini, S. H., Nenes, A., Carlton, A. G., Surratt, J. D., McNeill, V. F., and Pye, H. O. T. (2017). Simulating Aqueous-Phase Isoprene-Epoxydiol (IEPOX) Secondary Organic Aerosol Production During the 2013 Southern Oxidant and Aerosol Study (SOAS). *Environmental Science & Technology, 51*(9), 5026-5034. doi:10.1021/acs.est.6b05750

Buysse, C. E., Kaulfus, A., Nair, U., and Jaffe, D. A. (2019). Relationships between Particulate Matter, Ozone, and Nitrogen Oxides during Urban Smoke Events in the Western US. *Environmental Science & Technology, 53*(21), 12519-12528. doi:10.1021/acs.est.9b05241

Calvert, J. G., Bottenheim, J. W., and Strausz, O. P. (1978). MECHANISM OF THE HOMOGENEOUS OXIDATION OF SULFUR DIOXIDE IN THE TROPOSPHERE. In R. B. Husar, J. P. Lodge, & D. J. Moore (Eds.), *Sulfur in the Atmosphere* (pp. 197-226): Pergamon.

Campbell, J. R., Battaglia, M., Jr., Dingilian, K., Cesler-Maloney, M., St Clair, J. M., Hanisco, T. F., Robinson, E., DeCarlo, P., Simpson, W., Nenes, A., Weber, R. J., and Mao, J. (2022). Source and Chemistry of Hydroxymethanesulfonate (HMS) in Fairbanks, Alaska. *Environmental Science & Technology, 56*(12), 7657-7667. doi:10.1021/acs.est.2c00410

Chameides, W. L. (1984). The photochemistry of a remote marine stratiform cloud. *Journal of Geophysical Research: Atmospheres, 89*(D3), 4739-4755. doi:https://doi.org/10.1029/JD089iD03p04739

Chen, C., Zhu, P., Lan, L., Zhou, L., Liu, R., Sun, Q., Ban, J., Wang, W., Xu, D., and Li, T. (2018). Short-term exposures to PM2.5 and cause-specific mortality of cardiovascular health in China. *Environmental Research, 161*, 188-194. doi:https://doi.org/10.1016/j.envres.2017.10.046

Chen, D., Wang, Y., McElroy, M. B., He, K., Yantosca, R. M., and Le Sager, P. (2009). Regional CO pollution and export in China simulated by the high-resolution nested-grid GEOS-Chem model. *Atmos. Chem. Phys., 9*(11), 3825-3839. doi:10.5194/acp-9-3825-2009

Chen, T., Chu, B., Ge, Y., Zhang, S., Ma, Q., He, H., and Li, S.-M. (2019). Enhancement of aqueous sulfate formation by the coexistence of NO2/NH3 under high ionic strengths in aerosol water. *Environmental Pollution, 252*, 236-244. doi:https://doi.org/10.1016/j.envpol.2019.05.119

Cheng, Y., Zheng, G., Wei, C., Mu, Q., Zheng, B., Wang, Z., Gao, M., Zhang, Q., He, K., Carmichael, G., Pöschl, U., and Su, H. (2016). Reactive nitrogen chemistry in aerosol water as a source of sulfate during haze events in China. *Science Advances, 2*(12), e1601530. doi:10.1126/sciadv.1601530

Cho, S., Makar, P. A., Lee, W. S., Herage, T., Liggio, J., Li, S. M., Wiens, B., and Graham, L. (2009). Evaluation of a unified regional air-quality modeling system (AURAMS) using PrAIRie2005 field study data: The effects of

emissions data accuracy on particle sulphate predictions. *Atmospheric Environment, 43*(11), 1864-1877. doi:https://doi.org/10.1016/j.atmosenv.2008.12.048

Clements, A. L., Buzcu-Guven, B., Fraser, M. P., Kulkarni, P., and Chellam, S. (2013). Role of particulate metals in heterogenous secondary sulfate formation. *Atmospheric Environment, 75*, 233-240. doi:https://doi.org/10.1016/j.atmosenv.2013.04.038

Clifton, C. L., Altstein, N., and Huie, R. E. (1988). Rate constant for the reaction of nitrogen dioxide with sulfur(IV) over the pH range 5.3-13. *Environmental Science & Technology, 22*(5), 586-589. doi:10.1021/es00170a018

Deister, U., Neeb, R., Helas, G., and Warneck, P. (1986). Temperature dependence of the equilibrium CH2(OH)2 + HSO3- = CH2(OH)SO3- + H2O in aqueous solution. *The Journal of Physical Chemistry, 90*(14), 3213-3217. doi:10.1021/j100405a033

Dovrou, E., Lim, C. Y., Canagaratna, M. R., Kroll, J. H., Worsnop, D. R., and Keutsch, F. N. (2019). Measurement techniques for identifying and quantifying hydroxymethanesulfonate (HMS) in an aqueous matrix and particulate matter using aerosol mass spectrometry and ion chromatography. *Atmos. Meas. Tech., 12*(10), 5303-5315. doi:10.5194/amt-12-5303-2019

ECCC. (2022). *National Air Pollution Surveillance Program*. Retrieved from Government of Canada Open Data Portal: open.canada.ca

Eckhardt, S., Quennehen, B., Olivié, D. J. L., Berntsen, T. K., Cherian, R., Christensen, J. H., Collins, W., Crepinsek, S., Daskalakis, N., Flanner, M., Herber, A., Heyes, C., Hodnebrog, Ø., Huang, L., Kanakidou, M., Klimont, Z., Langner, J., Law, K. S., Lund, M. T., Mahmood, R., Massling, A., Myriokefalitakis, S., Nielsen, I. E., Nøjgaard, J. K., Quaas, J., Quinn, P. K., Raut, J. C., Rumbold, S. T., Schulz, M., Sharma, S., Skeie, R. B., Skov, H., Uttal, T., von Salzen, K., and Stohl, A. (2015). Current model capabilities for simulating black carbon and sulfate concentrations in the Arctic atmosphere: a multi-model evaluation using a comprehensive measurement data set. *Atmos. Chem. Phys., 15*(16), 9413-9433. doi:10.5194/acp-15-9413-2015

Elser, M., Huang, R. J., Wolf, R., Slowik, J. G., Wang, Q., Canonaco, F., Li, G., Bozzetti, C., Daellenbach, K. R., Huang, Y., Zhang, R., Li, Z., Cao, J., Baltensperger, U., El-Haddad, I., and Prévôt, A. S. H. (2016). New insights into PM2.5 chemical composition and sources in two major cities in China during extreme haze events using aerosol mass spectrometry. *Atmos. Chem. Phys., 16*(5), 3207-3225. doi:10.5194/acp-16-3207-2016

Ervens, B., Herckes, P., Feingold, G., Lee, T., Collett, J. L., and Kreidenweis, S. M. (2003). On the Drop-Size Dependence of Organic Acid and Formaldehyde Concentrations in Fog. *Journal of Atmospheric Chemistry, 46*(3), 239-269. doi:10.1023/A:1026393805907

Fahey, K. M., Carlton, A. G., Pye, H. O. T., Baek, J., Hutzell, W. T., Stanier, C. O., Baker, K. R., Appel, K. W., Jaoui, M., and Offenberg, J. H. (2017). A framework for expanding aqueous chemistry in the Community Multiscale Air Quality (CMAQ) model version 5.1. *Geosci. Model Dev., 10*(4), 1587-1605. doi:10.5194/gmd-10-1587-2017

Fahey, K. M., and Roselle, S. (2019, October 21 - 23, 2019). *Investigating aqueous production pathways of particulate sulfur in CMAQ with AQCHEM-KMT (version 2) and the sulfur tracking method.* Paper presented at the 2019 Annual CMAS Conference, Chapel Hill, NC.

Fan, M.-Y., Zhang, Y.-L., Lin, Y.-C., Li, J., Cheng, H., An, N., Sun, Y., Qiu, Y., Cao, F., and Fu, P. (2020). Roles of Sulfur Oxidation Pathways in the Variability in Stable Sulfur Isotopic Composition of Sulfate Aerosols at an Urban Site in Beijing, China. *Environmental Science & Technology Letters, 7*(12), 883-888. doi:10.1021/acs.estlett.0c00623

Fan, W., Chen, T., Zhu, Z., Zhang, H., Qiu, Y., and Yin, D. (2022). A review of secondary organic aerosols formation focusing on organosulfates and organic nitrates. *Journal of Hazardous Materials, 430*, 128406. doi:https://doi.org/10.1016/j.jhazmat.2022.128406

Fountoukis, C., and Nenes, A. (2007). ISORROPIA II: a computationally efficient thermodynamic equilibrium model for K^+–Ca^{2+}–Mg^{2+}–NH_4^+–Na^+–SO_4^{2-}–NO_3^-–Cl^-–H_2O aerosols. *Atmos. Chem. Phys., 7*(17), 4639-4659. doi:10.5194/acp-7-4639-2007

Gao, M., Carmichael, G. R., Wang, Y., Saide, P. E., Yu, M., Xin, J., Liu, Z., and Wang, Z. (2016). Modeling study of the 2010 regional haze event in the North China Plain. *Atmos. Chem. Phys., 16*(3), 1673-1691. doi:10.5194/acp-16-1673-2016

Gaudet, B. J. S., D. R. (2010). *Stable Boundary Layers Representation in Meteorological Models in Extremely Cold Wintertime Conditions*. Retrieved from https://dec.alaska.gov/media/7093/wrf-fairbanks-epafinalreport.pdf

Gaudet, B. J. S., D. R. (2012). *Fairbanks, North Star Borough AK PM2.5 Non-Attainment Area WRF-ARW*. Retrieved from https://dec.alaska.gov/media/7090/adec127617finalreport.pdf

Guenther, A. B., Jiang, X., Heald, C. L., Sakulyanontvittaya, T., Duhl, T., Emmons, L. K., and Wang, X. (2012). The Model of Emissions of Gases and Aerosols from Nature version 2.1 (MEGAN2.1): an extended and updated framework for modeling biogenic emissions. *Geosci. Model Dev., 5*(6), 1471-1492. doi:10.5194/gmd-5-1471-2012

Hanson, D. R., Ravishankara, A. R., and Solomon, S. (1994). Heterogeneous reactions in sulfuric acid aerosols: A framework for model calculations. *Journal of Geophysical Research: Atmospheres, 99*(D2), 3615-3629. doi:https://doi.org/10.1029/93JD02932

Hayes, R. B., Lim, C., Zhang, Y., Cromar, K., Shao, Y., Reynolds, H. R., Silverman, D. T., Jones, R. R., Park, Y., Jerrett, M., Ahn, J., and Thurston, G. D. (2020). PM2.5 air pollution and cause-specific cardiovascular disease mortality. *International Journal of Epidemiology, 49*(1), 25-35. doi:10.1093/ije/dyz114

Hoffmann, M. R., and Calvert, J. G. (1985). *Chemical Transformation Modules for Eulerian Acid Deposition Models*. Retrieved from US Environmental Protection Agency, Research Triangle Park, NC:

Holzworth, G. C. (1972). Vertical Temperature Structure During the 1966 Thanksgiving Week Air Pollution Episode in New York City. *Monthly Weather Review, 100*(6), 445-450. doi:https://doi.org/10.1175/1520-0493(1972)100<0445:VTSDTT>2.3.CO;2

Huang, L., Coddens, E. M., and Grassian, V. H. (2019). Formation of Organosulfur Compounds from Aqueous Phase Reactions of S(IV) with Methacrolein and Methyl Vinyl Ketone in the Presence of Transition Metal Ions. *ACS Earth and Space Chemistry, 3*(9), 1749-1755. doi:10.1021/acsearthspacechem.9b00173

Huang, L., Liu, T., and Grassian, V. H. (2020). Radical-Initiated Formation of Aromatic Organosulfates and Sulfonates in the Aqueous Phase. *Environmental Science & Technology, 54*(19), 11857-11864. doi:10.1021/acs.est.0c05644

Ibusuki, T., and Takeuchi, K. (1987). Sulfur dioxide oxidation by oxygen catalyzed by mixtures of manganese(II) and iron(III) in aqueous solutions at environmental reaction conditions. *Atmospheric Environment (1967), 21*(7), 1555-1560. doi:https://doi.org/10.1016/0004-6981(87)90317-9

IPCC. (2013). *IPCC, 2013: Summary for Policymakers. In: Climate Change 2013: The Physical Science Basis. Contribution of Working Group I to the Fifth Assessment*

Report of the Intergovernmental Panel on Climate Change. Retrieved from Cambridge University Press, Cambridge, United Kingdom and New York, NY, USA:

Jacob, D. J. (2000). Heterogeneous chemistry and tropospheric ozone. *Atmospheric Environment, 34*(12), 2131-2159. doi:https://doi.org/10.1016/S1352-2310(99)00462-8

Janssens-Maenhout, G., Crippa, M., Guizzardi, D., Dentener, F., Muntean, M., Pouliot, G., Keating, T., Zhang, Q., Kurokawa, J., Wankmüller, R., Denier van der Gon, H., Kuenen, J. J. P., Klimont, Z., Frost, G., Darras, S., Koffi, B., and Li, M. (2015). HTAP_v2.2: a mosaic of regional and global emission grid maps for 2008 and 2010 to study hemispheric transport of air pollution. *Atmos. Chem. Phys., 15*(19), 11411-11432. doi:10.5194/acp-15-11411-2015

Kemball-Cook, S., Jia, Y., Emery, C., and Morris, R. (2005). *Alaska MM5 Modeling for the 2002 Annual Period to Support Visibility Modeling*. Retrieved from Novato, CA: http://pah.cert.ucr.edu/aqm/308/docs/alaska/Alaska_MM5_DraftReport_Sept05.pdf

Kim, Y. P., Pun, B. K. L., Chan, C. K., Flagan, R. C., and Seinfeld, J. H. (1994). Determination of Water Activity in Ammonium Sulfate and Sulfuric Acid Mixtures Using Levitated Single Particles. *Aerosol Science and Technology, 20*(3), 275-284. doi:10.1080/02786829408959683

Kok, G. L., Gitlin, S. N., and Lazrus, A. L. (1986). Kinetics of the formation and decomposition of hydroxymethanesulfonate. *Journal of Geophysical Research: Atmospheres, 91*(D2), 2801-2804. doi:https://doi.org/10.1029/JD091iD02p02801

Kosak-Channing, L. F., and Helz, G. R. (1983). Solubility of ozone in aqueous solutions of 0-0.6 M ionic strength at 5-30.degree.C. *Environmental Science & Technology, 17*(3), 145-149. doi:10.1021/es00109a005

Kovacs, K., McIlwaine, R., Gannon, K., Taylor, A. F., and Scott, S. K. (2005). Complex Behavior in the Formaldehyde−Sulfite Reaction. *The Journal of Physical Chemistry A, 109*(1), 283-288. doi:10.1021/jp0464324

Lagrange, J., Pallares, C., and Lagrange, P. (1994). Electrolyte effects on aqueous atmospheric oxidation of sulphur dioxide by ozone. *Journal of Geophysical Research: Atmospheres, 99*(D7), 14595-14600. doi:https://doi.org/10.1029/94JD00573

Lee, Y., and Schwartz, S. E. (1983a). Kinetics of oxidation of aqueous sulfur (IV) by nitrogen dioxide. *Precipitation Scavenging, Dry Deposition and Resuspension, 1*, 453-470.

Lee, Y. N., and Schwartz, S. E. (1983b). Kinetics of Oxidation of Aqueous Sulfur(IV) by Nitrogen Dioxide. In e. Pruppacher et al. (Ed.), *Precipitation, Scavenging, Dry Deposition and Resuspension* (Vol. 1). New York: Elsevier.

Li, H., Zhang, Q., Zhang, Q., Chen, C., Wang, L., Wei, Z., Zhou, S., Parworth, C., Zheng, B., Canonaco, F., Prévôt, A. S. H., Chen, P., Zhang, H., Wallington, T. J., and He, K. (2017). Wintertime aerosol chemistry and haze evolution in an extremely polluted city of the North China Plain: significant contribution from coal and biomass combustion. *Atmos. Chem. Phys., 17*(7), 4751-4768. doi:10.5194/acp-17-4751-2017

Li, J., Zhang, Y.-L., Cao, F., Zhang, W., Fan, M., Lee, X., and Michalski, G. (2020). Stable Sulfur Isotopes Revealed a Major Role of Transition-Metal Ion-Catalyzed SO2 Oxidation in Haze Episodes. *Environmental Science & Technology, 54*(5), 2626-2634. doi:10.1021/acs.est.9b07150

Li, M., Su, H., Zheng, G., Kuhn, U., Kim, N., Li, G., Ma, N., Pöschl, U., and Cheng, Y. (2022). Aerosol pH and Ion Activities of HSO4– and SO42– in Supersaturated Single Droplets. *Environmental Science & Technology, 56*(18), 12863-12872. doi:10.1021/acs.est.2c01378

Lide, D. R., Frederikse, H. P. R., and (Eds.). (1995). *CRC Handbook of Chemistry and Physics* (D. R. Lide & H. P. R. Frederikse Eds. 76 ed.). Boca Raton, Fl: CRC Press, Inc.

Liggio, J., Li, S.-M., Hayden, K., Taha, Y. M., Stroud, C., Darlington, A., Drollette, B. D., Gordon, M., Lee, P., Liu, P., Leithead, A., Moussa, S. G., Wang, D., O'Brien, J., Mittermeier, R. L., Brook, J. R., Lu, G., Staebler, R. M., Han, Y., Tokarek, T. W., Osthoff, H. D., Makar, P. A., Zhang, J., L. Plata, D., and Gentner, D. R. (2016). Oil sands operations as a large source of secondary organic aerosols. *Nature, 534*(7605), 91-94. doi:10.1038/nature17646

Lind, J. A., Lazrus, A. L., and Kok, G. L. (1987). Aqueous phase oxidation of sulfur(IV) by hydrogen peroxide, methylhydroperoxide, and peroxyacetic acid. *Journal of Geophysical Research: Atmospheres, 92*(D4), 4171-4177. doi:https://doi.org/10.1029/JD092iD04p04171

Littlejohn, D., Wang, Y., and Chang, S. G. (1993). Oxidation of aqueous sulfite ion by nitrogen dioxide. *Environmental Science & Technology, 27*(10), 2162-2167. doi:10.1021/es00047a024

Liu, L., Li, W., Lin, Q., Wang, Y., Zhang, J., Zhu, Y., Yuan, Q., Zhou, S., Zhang, D., Baldo, C., and Shi, Z. (2022). Size-dependent aerosol iron solubility in an urban atmosphere. *npj Climate and Atmospheric Science, 5*(1), 53. doi:10.1038/s41612-022-00277-z

Liu, T., Clegg, S. L., and Abbatt, J. P. D. (2020). Fast oxidation of sulfur dioxide by hydrogen peroxide in deliquesced aerosol particles. *Proceedings of the National Academy of Sciences, 117*(3), 1354. doi:10.1073/pnas.1916401117

Luecken, D. J., Yarwood, G., and Hutzell, W. T. (2019). Multipollutant modeling of ozone, reactive nitrogen and HAPs across the continental US with CMAQ-CB6. *Atmospheric Environment, 201*, 62-72. doi:https://doi.org/10.1016/j.atmosenv.2018.11.060

Ma, T., Furutani, H., Duan, F., Kimoto, T., Jiang, J., Zhang, Q., Xu, X., Wang, Y., Gao, J., Geng, G., Li, M., Song, S., Ma, Y., Che, F., Wang, J., Zhu, L., Huang, T., Toyoda, M., and He, K. (2020). Contribution of hydroxymethanesulfonate (HMS) to severe winter haze in the North China Plain. *Atmos. Chem. Phys., 20*(10), 5887-5897. doi:10.5194/acp-20-5887-2020

Maahs, H. G. (1983). Kinetics and mechanism of the oxidation of S(IV) by ozone in aqueous solution with particular reference to SO2 conversion in nonurban tropospheric clouds. *Journal of Geophysical Research: Oceans, 88*(C15), 10721-10732. doi:https://doi.org/10.1029/JC088iC15p10721

Maaß, F., Elias, H., and Wannowius, K. J. (1999). Kinetics of the oxidation of hydrogen sulfite by hydrogen peroxide in aqueous solution:: ionic strength effects and temperature dependence. *Atmospheric Environment, 33*(27), 4413-4419. doi:https://doi.org/10.1016/S1352-2310(99)00212-5

Malek, E., Davis, T., Martin, R. S., and Silva, P. J. (2006). Meteorological and environmental aspects of one of the worst national air pollution episodes (January, 2004) in Logan, Cache Valley, Utah, USA. *Atmospheric Research, 79*(2), 108-122. doi:https://doi.org/10.1016/j.atmosres.2005.05.003

980   Malingowski, J., Atkinson, D., Fochesatto, J., Cherry, J., and Stevens, E. (2014). An observational study of radiation temperature inversions in Fairbanks, Alaska. *Polar Science, 8*(1), 24-39. doi:https://doi.org/10.1016/j.polar.2014.01.002

Marais, E. A., Jacob, D. J., Jimenez, J. L., Campuzano-Jost, P., Day, D. A., Hu, W., Krechmer, J., Zhu, L., Kim, P. S., Miller, C. C., Fisher, J. A., Travis, K., Yu, K., Hanisco, T. F., Wolfe, G. M., Arkinson, H. L., Pye, H. O. T., Froyd,
985   K. D., Liao, J., and McNeill, V. F. (2016). Aqueous-phase mechanism for secondary organic aerosol formation from isoprene: application to the southeast United States and co-benefit of SO2 emission controls. *Atmos. Chem. Phys., 16*(3), 1603-1618. doi:10.5194/acp-16-1603-2016

Martin, L. R. (1984). Kinetic studies of sulfite oxidation in aqueous solution in SO2, NO and NO2 Oxidation Mechanisms: Atmospheric Considerations. In J. G. Calvert (Ed.), (pp. 63-100). Butterworths, London.
990   Martin, L. R., and Good, T. W. (1991). Catalyzed oxidation of sulfur dioxide in solution: The iron-manganese synergism. *Atmospheric Environment. Part A. General Topics, 25*(10), 2395-2399. doi:https://doi.org/10.1016/0960-1686(91)90113-L

Martin, L. R., and Hill, M. W. (1967). The iron catalyzed oxidation of sulfur: Reconciliation of the literature rates. *Atmospheric Environment (1967), 21*(6), 1487-1490. doi:https://doi.org/10.1016/0004-6981(67)90100-X
995   Martin, R. L., and Hill, M. W. (1987). The effect of ionic strength on the manganese catalyzed oxidation of sulfur(IV). *Atmospheric Environment (1967), 21*(10), 2267-2270. doi:https://doi.org/10.1016/0004-6981(87)90361-1

Mathur, R., Xing, J., Gilliam, R., Sarwar, G., Hogrefe, C., Pleim, J., Pouliot, G., Roselle, S., Spero, T. L., Wong, D. C., and Young, J. (2017). Extending the Community Multiscale Air Quality (CMAQ) modeling system to hemispheric scales: overview of process considerations and initial applications. *Atmos. Chem. Phys., 17*(20), 12449-12474.
1000   doi:10.5194/acp-17-12449-2017

Mayfield, J. A., and Fochesatto, G. J. (2013). The Layered Structure of the Winter Atmospheric Boundary Layer in the Interior of Alaska. *Journal of Applied Meteorology and Climatology, 52*(4), 953-973. doi:https://doi.org/10.1175/JAMC-D-12-01.1

McArdle, J. V., and Hoffmann, M. R. (1983). Kinetics and mechanism of the oxidation of aquated sulfur dioxide by
1005   hydrogen peroxide at low pH. *The Journal of Physical Chemistry, 87*(26), 5425-5429. doi:10.1021/j150644a024

McLaughlin, J. C., L. (2010). *Association between Air Quality and Hospital Visits — Fairbanks, 2003–2008*. Retrieved from Anchorage, AK:

Mekic, M., and Gligorovski, S. (2021). Ionic strength effects on heterogeneous and multiphase chemistry: Clouds versus aerosol particles. *Atmospheric Environment, 244*, 117911. doi:https://doi.org/10.1016/j.atmosenv.2020.117911
1010   Millero, F. J., Hershey, J. P., Johnson, G., and Zhang, J.-Z. (1989). The solubility of SO2 and the dissociation of H2SO3 in NaCl solutions. *Journal of Atmospheric Chemistry, 8*(4), 377-389. doi:10.1007/BF00052711

Moch, J. M., Dovrou, E., Mickley, L. J., Keutsch, F. N., Cheng, Y., Jacob, D. J., Jiang, J., Li, M., Munger, J. W., Qiao, X., and Zhang, Q. (2018). Contribution of Hydroxymethane Sulfonate to Ambient Particulate Matter: A Potential Explanation for High Particulate Sulfur During Severe Winter Haze in Beijing. *Geophysical Research Letters,*
1015   *45*(21), 11,969-911,979. doi:https://doi.org/10.1029/2018GL079309

Moch, J. M., Dovrou, E., Mickley, L. J., Keutsch, F. N., Liu, Z., Wang, Y., Dombek, T. L., Kuwata, M., Budisulistiorini, S. H., Yang, L., Decesari, S., Paglione, M., Alexander, B., Shao, J., Munger, J. W., and Jacob, D. J. (2020). Global Importance of Hydroxymethanesulfonate in Ambient Particulate Matter: Implications for Air Quality. *Journal of Geophysical Research: Atmospheres, 125*(18), e2020JD032706. doi:https://doi.org/10.1029/2020JD032706
1020   Nakanishi, M., and Niino, H. (2009). Development of an improved turbulence closure model for the atmospheric boundary layer. *Journal of the Meteorological Society of Japan. Ser. II, 87*(5), 895-912.

Nguyen, T. K. V., Petters, M. D., Suda, S. R., Guo, H., Weber, R. J., and Carlton, A. G. (2014). Trends in particle-phase liquid water during the Southern Oxidant and Aerosol Study. *Atmos. Chem. Phys., 14*(20), 10911-10930. doi:10.5194/acp-14-10911-2014
1025   O'Sullivan, D. W., Lee, M., Noone, B. C., and Heikes, B. G. (1996). Henry's Law Constant Determinations for Hydrogen Peroxide, Methyl Hydroperoxide, Hydroxymethyl Hydroperoxide, Ethyl Hydroperoxide, and Peroxyacetic Acid. *The Journal of Physical Chemistry, 100*(8), 3241-3247. doi:10.1021/jp951168n

Olson, T. M., and Hoffmann, M. R. (1986). On the kinetics of formaldehyde-S(IV) adduct formation in slightly acidic solution. *Atmospheric Environment (1967), 20*(11), 2277-2278. doi:https://doi.org/10.1016/0004-6981(86)90318-5

1030   Otte, T. L., and Pleim, J. E. (2010). The Meteorology-Chemistry Interface Processor (MCIP) for the CMAQ modeling system: updates through MCIPv3.4.1. *Geosci. Model Dev., 3*(1), 243-256. doi:10.5194/gmd-3-243-2010

Pandis, S. N., and Seinfeld, J. H. (1989). Sensitivity analysis of a chemical mechanism for aqueous-phase atmospheric chemistry. *Journal of Geophysical Research: Atmospheres, 94*(D1), 1105-1126. doi:https://doi.org/10.1029/JD094iD01p01105

1035   Peng, J., Hu, M., Shang, D., Wu, Z., Du, Z., Tan, T., Wang, Y., Zhang, F., and Zhang, R. (2021). Explosive Secondary Aerosol Formation during Severe Haze in the North China Plain. *Environmental Science & Technology, 55*(4), 2189-2207. doi:10.1021/acs.est.0c07204

Petters, M. D., and Kreidenweis, S. M. (2007). A single parameter representation of hygroscopic growth and cloud condensation nucleus activity. *Atmos. Chem. Phys., 7*(8), 1961-1971. doi:10.5194/acp-7-1961-2007

1040   Pye, H. O. T., Murphy, B. N., Xu, L., Ng, N. L., Carlton, A. G., Guo, H., Weber, R., Vasilakos, P., Appel, K. W., Budisulistiorini, S. H., Surratt, J. D., Nenes, A., Hu, W., Jimenez, J. L., Isaacman-VanWertz, G., Misztal, P. K., and Goldstein, A. H. (2017). On the implications of aerosol liquid water and phase separation for organic aerosol mass. *Atmos. Chem. Phys., 17*(1), 343-369. doi:10.5194/acp-17-343-2017

Pye, H. O. T., Nenes, A., Alexander, B., Ault, A. P., Barth, M. C., Clegg, S. L., Collett Jr, J. L., Fahey, K. M., Hennigan, C. 1045   J., Herrmann, H., Kanakidou, M., Kelly, J. T., Ku, I. T., McNeill, V. F., Riemer, N., Schaefer, T., Shi, G., Tilgner, A., Walker, J. T., Wang, T., Weber, R., Xing, J., Zaveri, R. A., and Zuend, A. (2020). The acidity of atmospheric particles and clouds. *Atmos. Chem. Phys., 20*(8), 4809-4888. doi:10.5194/acp-20-4809-2020

Queally, J. (2016). The blaze that won't die: How Monterey County wildfire became one of costliest to fight. *Los Angeles Times*. Retrieved from https://www.latimes.com/local/lanow/la-me-ln-soberanes-fire-20160926-snap-1050   htmlstory.html

Rao, X., and Collett, J. L. (1998). The Drop Size-Dependence of Iron and Manganese Concentrations in Clouds and Fogs: Implications for Sulfate Production. *Journal of Atmospheric Chemistry, 30*(2), 273-289. doi:10.1023/A:1006044614291

Sander, R. (2015). Compilation of Henry's law constants (version 4.0) for water as solvent. *Atmos. Chem. Phys., 15*(8), 4399-1055   4981. doi:10.5194/acp-15-4399-2015

Sarwar, G., Fahey, K., Kwok, R., Gilliam, R. C., Roselle, S. J., Mathur, R., Xue, J., Yu, J., and Carter, W. P. L. (2013). Potential impacts of two SO2 oxidation pathways on regional sulfate concentrations: Aqueous-phase oxidation by NO2 and gas-phase oxidation by Stabilized Criegee Intermediates. *Atmospheric Environment, 68*, 186-197. doi:https://doi.org/10.1016/j.atmosenv.2012.11.036

1060   Schwartz, S. E. (1986, 1986//). *Mass-Transport Considerations Pertinent to Aqueous Phase Reactions of Gases in Liquid-Water Clouds.* Paper presented at the Chemistry of Multiphase Atmospheric Systems, Berlin, Heidelberg.

Schwartz, S. E., and Freiberg, J. E. (1981). Mass-transport limitation to the rate of reaction of gases in liquid droplets: Application to oxidation of SO2 in aqueous solutions. *Atmospheric Environment (1967), 15*(7), 1129-1144. doi:https://doi.org/10.1016/0004-6981(81)90303-6

1065   Scott, J. A. (1953). Fog and deaths in London, December 1952. *Public Health Rep (1896), 68*(5), 474-479.

Seinfeld, J. H., and Pandis, S. N. (2016). Atmospheric Chemistry and Physics: From Air Pollution to Climate Change. In (Vol. Third Edition, pp. 288-289). Hoboken, New Jersey: John Wiley & Sons, Inc.

Shao, J., Chen, Q., Wang, Y., Lu, X., He, P., Sun, Y., Shah, V., Martin, R. V., Philip, S., Song, S., Zhao, Y., Xie, Z., Zhang, L., and Alexander, B. (2019). Heterogeneous sulfate aerosol formation mechanisms during wintertime Chinese haze 1070   events: air quality model assessment using observations of sulfate oxygen isotopes in Beijing. *Atmos. Chem. Phys., 19*(9), 6107-6123. doi:10.5194/acp-19-6107-2019

Silva, R. A., Adelman, Z., Fry, M. M., and West, J. J. (2016). The Impact of Individual Anthropogenic Emissions Sectors on the Global Burden of Human Mortality due to Ambient Air Pollution. *Environmental Health Perspectives, 124*(11), 1776-1784. doi:10.1289/EHP177

1075   Simpson, W. R., Mao, J., Fochesatto, G. J., Law, K. S., DeCarlo, P. F., Schmale, J., Pratt, K. A., Arnold, S. R., Stutz, J., Dibb, J. E., Creamean, J. M., Weber, R. J., Williams, B. J., Alexander, B., Hu, L., Yokelson, R. J., Shiraiwa, M., Decesari, S., Anastasio, C., D'Anna, B., Gilliam, R. C., Nenes, A., St. Clair, J. M., Trost, B., Flynn, J. H., Savarino, J., Conner, L. D., Kettle, N., Heeringa, K. M., Albertin, S., Baccarini, A., Barret, B., Battaglia, M. A., Bekki, S., Brado, T. J., Brett, N., Brus, D., Campbell, J. R., Cesler-Maloney, M., Cooperdock, S., Cysneiros de Carvalho, K.,

Delbarre, H., DeMott, P. J., Dennehy, C. J. S., Dieudonné, E., Dingilian, K. K., Donateo, A., Doulgeris, K. M., Edwards, K. C., Fahey, K., Fang, T., Guo, F., Heinlein, L. M. D., Holen, A. L., Huff, D., Ijaz, A., Johnson, S., Kapur, S., Ketcherside, D. T., Levin, E., Lill, E., Moon, A. R., Onishi, T., Pappaccogli, G., Perkins, R., Pohorsky, R., Raut, J.-C., Ravetta, F., Roberts, T., Robinson, E. S., Scoto, F., Selimovic, V., Sunday, M. O., Temime-Roussel, B., Tian, X., Wu, J., and Yang, Y. (2024). Overview of the Alaskan Layered Pollution and Chemical Analysis (ALPACA) Field Experiment. *ACS ES&T Air, 1*(3), 200-222. doi:10.1021/acsestair.3c00076

Skamarock, W. C., Klemp, J. B., Dudhia, J., Gill, D. O., Barker, D. M., Duda, M. G., Huang, X.-Y., Wang, W., and Powers, J. G. (2008). A description of the advanced research WRF version 3. *NCAR technical note, 475*, 113.

Snider, G., Weagle, C. L., Murdymootoo, K. K., Ring, A., Ritchie, Y., Stone, E., Walsh, A., Akoshile, C., Anh, N. X., Balasubramanian, R., Brook, J., Qonitan, F. D., Dong, J., Griffith, D., He, K., Holben, B. N., Kahn, R., Lagrosas, N., Lestari, P., Ma, Z., Misra, A., Norford, L. K., Quel, E. J., Salam, A., Schichtel, B., Segev, L., Tripathi, S., Wang, C., Yu, C., Zhang, Q., Zhang, Y., Brauer, M., Cohen, A., Gibson, M. D., Liu, Y., Martins, J. V., Rudich, Y., and Martin, R. V. (2016). Variation in global chemical composition of PM2.5: emerging results from SPARTAN. *Atmos. Chem. Phys., 16*(15), 9629-9653. doi:10.5194/acp-16-9629-2016

Song, H., Lu, K., Ye, C., Dong, H., Li, S., Chen, S., Wu, Z., Zheng, M., Zeng, L., Hu, M., and Zhang, Y. (2021b). A comprehensive observation-based multiphase chemical model analysis of sulfur dioxide oxidations in both summer and winter. *Atmos. Chem. Phys., 21*(17), 13713-13727. doi:10.5194/acp-21-13713-2021

Song, S., Gao, M., Xu, W., Sun, Y., Worsnop, D. R., Jayne, J. T., Zhang, Y., Zhu, L., Li, M., Zhou, Z., Cheng, C., Lv, Y., Wang, Y., Peng, W., Xu, X., Lin, N., Wang, Y., Wang, S., Munger, J. W., Jacob, D. J., and McElroy, M. B. (2019). Possible heterogeneous chemistry of hydroxymethanesulfonate (HMS) in northern China winter haze. *Atmos. Chem. Phys., 19*(2), 1357-1371. doi:10.5194/acp-19-1357-2019

Song, S., Ma, T., Zhang, Y., Shen, L., Liu, P., Li, K., Zhai, S., Zheng, H., Gao, M., Moch, J. M., Duan, F., He, K., and McElroy, M. B. (2021a). Global modeling of heterogeneous hydroxymethanesulfonate chemistry. *Atmos. Chem. Phys., 21*(1), 457-481. doi:10.5194/acp-21-457-2021

Staudinger, J., and Roberts, P. V. (1996). A critical review of Henry's law constants for environmental applications. *Critical Reviews in Environmental Science and Technology, 26*(3), 205-297. doi:10.1080/10643389609388492

Stroud, C. M., Paul; Moran, Michael; Gong, Wanmin; Gong, Sunling; Zhang, Junhua; Brook, Jeff; Bouchet, Veronique. (2009). *ANTHROPOGENIC IMPACTS ON ORGANIC AEROSOL: REGIONAL AIR QUALITY MODELING RESULTS FROM THE 2007 BAQS-MET FIELD STUDY*. Paper presented at the 8th Annual CMAS Conference, Chapel Hill. https://www.cmascenter.org/conference/2009/abstracts/stroud_anthropogenic_impacts_2009.pdf

Sun, Y., Wang, Z., Fu, P., Jiang, Q., Yang, T., Li, J., and Ge, X. (2013). The impact of relative humidity on aerosol composition and evolution processes during wintertime in Beijing, China. *Atmospheric Environment, 77*, 927-934. doi:https://doi.org/10.1016/j.atmosenv.2013.06.019

Surratt, J. D., Chan, A. W. H., Eddingsaas, N. C., Chan, M., Loza, C. L., Kwan, A. J., Hersey, S. P., Flagan, R. C., Wennberg, P. O., and Seinfeld, J. H. (2010). Reactive intermediates revealed in secondary organic aerosol formation from isoprene. *Proceedings of the National Academy of Sciences, 107*(15), 6640-6645. doi:doi:10.1073/pnas.0911114107

Tørseth, K., Aas, W., Breivik, K., Fjæraa, A. M., Fiebig, M., Hjellbrekke, A. G., Lund Myhre, C., Solberg, S., and Yttri, K. E. (2012). Introduction to the European Monitoring and Evaluation Programme (EMEP) and observed atmospheric composition change during 1972–2009. *Atmos. Chem. Phys., 12*(12), 5447-5481. doi:10.5194/acp-12-5447-2012

Tran, H. M., N. (2011). *Assessment of the Contribution of Traffic Emissions to the Mobile Vehicle Measured PM2.5 Concentration by Means of WRF-CMAQ Simulations*. Retrieved from Fairbanks, AK:

USEPA. Air Quality System Data Mart [internet database]. Retrieved from https://www.epa.gov/outdoor-air-quality-data. Retrieved 2022 https://www.epa.gov/outdoor-air-quality-data

USEPA. (2019). *Integrated Science Assessment (ISA) for Particulate Matter (Final Report, Dec 2019)* (EPA/600/R-19/188). Retrieved from Washington, DC: https://assessments.epa.gov/risk/document/&deid=347534

USEPA. (2020). CMAQ (5.3.2). Zenodo: USEPA Office of Research and Development.

USEPA. (2021). *EQUATESv1.0: Emissions, WRF/MCIP, CMAQv5.3.2 Data -- 2002-2019 US_12km and NHEMI_108km*. Retrieved from: https://doi.org/10.15139/S3/F2KJSK

1130   Wallace, J., and Kanaroglou, P. (2009). The effect of temperature inversions on ground-level nitrogen dioxide (NO2) and fine particulate matter (PM2.5) using temperature profiles from the Atmospheric Infrared Sounder (AIRS). *Science of The Total Environment, 407*(18), 5085-5095. doi:https://doi.org/10.1016/j.scitotenv.2009.05.050

Wang, G., Zhang, R., Gomez Mario, E., Yang, L., Levy Zamora, M., Hu, M., Lin, Y., Peng, J., Guo, S., Meng, J., Li, J., Cheng, C., Hu, T., Ren, Y., Wang, Y., Gao, J., Cao, J., An, Z., Zhou, W., Li, G., Wang, J., Tian, P., Marrero-Ortiz,
1135   W., Secrest, J., Du, Z., Zheng, J., Shang, D., Zeng, L., Shao, M., Wang, W., Huang, Y., Wang, Y., Zhu, Y., Li, Y., Hu, J., Pan, B., Cai, L., Cheng, Y., Ji, Y., Zhang, F., Rosenfeld, D., Liss Peter, S., Duce Robert, A., Kolb Charles, E., and Molina Mario, J. (2016). Persistent sulfate formation from London Fog to Chinese haze. *Proceedings of the National Academy of Sciences, 113*(48), 13630-13635. doi:10.1073/pnas.1616540113

Wang, J., Li, J., Ye, J., Zhao, J., Wu, Y., Hu, J., Liu, D., Nie, D., Shen, F., Huang, X., Huang, D. D., Ji, D., Sun, X., Xu, W.,
1140   Guo, J., Song, S., Qin, Y., Liu, P., Turner, J. R., Lee, H. C., Hwang, S., Liao, H., Martin, S. T., Zhang, Q., Chen, M., Sun, Y., Ge, X., and Jacob, D. J. (2020). Fast sulfate formation from oxidation of SO2 by NO2 and HONO observed in Beijing haze. *Nature Communications, 11*(1), 2844. doi:10.1038/s41467-020-16683-x

Wang, W., Liu, M., Wang, T., Song, Y., Zhou, L., Cao, J., Hu, J., Tang, G., Chen, Z., Li, Z., Xu, Z., Peng, C., Lian, C., Chen, Y., Pan, Y., Zhang, Y., Sun, Y., Li, W., Zhu, T., Tian, H., and Ge, M. (2021). Sulfate formation is dominated
1145   by manganese-catalyzed oxidation of SO2 on aerosol surfaces during haze events. *Nature Communications, 12*(1), 1993. doi:10.1038/s41467-021-22091-6

Wang, Y., Zhang, Q., Jiang, J., Zhou, W., Wang, B., He, K., Duan, F., Zhang, Q., Philip, S., and Xie, Y. (2014). Enhanced sulfate formation during China's severe winter haze episode in January 2013 missing from current models. *Journal of Geophysical Research: Atmospheres, 119*(17), 10,425-410,440. doi:https://doi.org/10.1002/2013JD021426
1150   Wiedinmyer, C., Akagi, S. K., Yokelson, R. J., Emmons, L. K., Al-Saadi, J. A., Orlando, J. J., and Soja, A. J. (2011). The Fire INventory from NCAR (FINN): a high resolution global model to estimate the emissions from open burning. *Geosci. Model Dev., 4*(3), 625-641. doi:10.5194/gmd-4-625-2011

Xing, J., Wang, J., Mathur, R., Wang, S., Sarwar, G., Pleim, J., Hogrefe, C., Zhang, Y., Jiang, J., Wong, D. C., and Hao, J. (2017). Impacts of aerosol direct effects on tropospheric ozone through changes in atmospheric dynamics and
1155   photolysis rates. *Atmos Chem Phys, 17*(16), 9869-9883. doi:10.5194/acp-17-9869-2017

Yang, J., Li, L., Wang, S., Li, H., Francisco, J. S., Zeng, X. C., and Gao, Y. (2019). Unraveling a New Chemical Mechanism of Missing Sulfate Formation in Aerosol Haze: Gaseous NO2 with Aqueous HSO3–/SO32–. *Journal of the American Chemical Society, 141*(49), 19312-19320. doi:10.1021/jacs.9b08503

Yang, X., Zhang, L., Chen, X., Liu, F., Shan, A., Liang, F., Li, X., Wu, H., Yan, M., Ma, Z., Dong, G., Liu, Y., Chen, J.,
1160   Wang, T., Zhao, B., Liu, Y., Gu, D., and Tang, N. (2021). Long-term exposure to ambient PM2.5 and stroke mortality among urban residents in northern China. *Ecotoxicology and Environmental Safety, 213*, 112063. doi:https://doi.org/10.1016/j.ecoenv.2021.112063

Yitshak-Sade, M., Bobb, J. F., Schwartz, J. D., Kloog, I., and Zanobetti, A. (2018). The association between short and long-term exposure to PM2.5 and temperature and hospital admissions in New England and the synergistic effect of the
1165   short-term exposures. *Science of The Total Environment, 639*, 868-875. doi:https://doi.org/10.1016/j.scitotenv.2018.05.181

Zhang, S., Sarwar, G., Xing, J., Chu, B., Xue, C., Sarav, A., Ding, D., Zheng, H., Mu, Y., Duan, F., Ma, T., and He, H. (2021b). Improving the representation of HONO chemistry in CMAQ and examining its impact on haze over China. *Atmos. Chem. Phys., 21*(20), 15809-15826. doi:10.5194/acp-21-15809-2021
1170   Zhang, T., Shen, Z. X., Su, H., Liu, S. X., Zhou, J. M., Zhao, Z. Z., Wang, Q. Y., Prévôt, A. S. H., and Cao, J. J. (2021a). Effects of Aerosol Water Content on the formation of secondary inorganic aerosol during a Winter Heavy PM2.5 Pollution Episode in Xi'an, China. *Atmospheric Environment, 252*, 118304. doi:https://doi.org/10.1016/j.atmosenv.2021.118304

Zheng, B., Zhang, Q., Zhang, Y., He, K. B., Wang, K., Zheng, G. J., Duan, F. K., Ma, Y. L., and Kimoto, T. (2015).
1175   Heterogeneous chemistry: a mechanism missing in current models to explain secondary inorganic aerosol formation during the January 2013 haze episode in North China. *Atmos. Chem. Phys., 15*(4), 2031-2049. doi:10.5194/acp-15-2031-2015

Zuend, A., Marcolli, C., Booth, A. M., Lienhard, D. M., Soonsin, V., Krieger, U. K., Topping, D. O., McFiggans, G., Peter, T., and Seinfeld, J. H. (2011). New and extended parameterization of the thermodynamic model AIOMFAC:

1180   calculation of activity coefficients for organic-inorganic mixtures containing carboxyl, hydroxyl, carbonyl, ether, ester, alkenyl, alkyl, and aromatic functional groups. *Atmos. Chem. Phys., 11*(17), 9155-9206. doi:10.5194/acp-11-9155-2011

        Zuend, A., and Seinfeld, J. H. (2012). Modeling the gas-particle partitioning of secondary organic aerosol: the importance of liquid-liquid phase separation. *Atmos. Chem. Phys., 12*(9), 3857-3882. doi:10.5194/acp-12-3857-2012

1185